Charged Particle Energization from Solar Winds

APPROVED BY

SUPERVISING COMMITTEE:

Wendell Horton, Supervisor

Gary Hallock, Supervisor

Charged Particle Energization from Solar Winds

by

Wei-Tai Lin, B.S.

THESIS

Presented to the Faculty of the Graduate School of

The University of Texas at Austin

in Partial Fulfillment

of the Requirements

for the Degree of

MASTER OF SCIENCE

THE UNIVERSITY OF TEXAS AT AUSTIN

May 2003

Dedicated to my family.

Acknowledgments

I would like to express my appreciation to my advisors, Professor W. Horton and Professor G. Hallock, for their many suggestions in connection with this thesis. And I really appreciate that Dr. Horton gives me a chance to do research related to space science. I also want to thank the multitudes of people who helped me, especially C. Crabtree. He taught me a lot of skills in softwares and numerical simulations.

This thesis is dedicated to my family for their support and patient encouragement.

Charged Particle Energization from Solar Winds

Wei-Tai Lin, M.S.
The University of Texas at Austin, 2003

Supervisors: Wendell Horton
Gary Hallock

Abstract

This thesis researches on the energy gain mechanism of charged particles in the Earth's magnetosphere. Particles coming from solar wind pass by the nose of the magnetosphere. When particles arrive in the tail region along the magnetopause they enter the Earth's magnetosphere through reconnection and generate the tail current. The solar wind leads to produce the electric field across the magnetic field in the geotail of the Earth. According to Faraday's law under steady state there exists an electric field E_y and E_y is the same everywhere in the geomagnetic tail. Energy acquired by the charged particles drifting in the space comes from the electric field because the magnetic field does not do work on the particles. The same type of the energizing processes in Earth's magnetotail occurs on the Sun during the solar coronal mass ejections. The Sun is the source of high energy protons and electrons. The relativistic

ions and electrons produced in the corona are released into the heliosphere.

The approach used to simulate the behaviors of particles is to integrate the equations of motions. In space the universal gravitation force of attraction on the particles is really small because of the small masses involved. The interaction of particles is through the Lorentz force from the electric and magnetic fields. The electric and magnetic fields are produced by a complex interaction of the solar wind plasma and the Earth's intrinsic magnetic field. These fields are well known from thirty years of space craft measurements during all types of space weather. Given the fields the Lorentz force with Newton's law determine the motion of charged particles in the Earth's magnetosphere. We can analyze the behaviors and properties of particles by integrating the Lorentz force equation. The magnetic field model we work with is the Tsyganenko 96 model (http://nssdc.gsfc.nasa.gov/space/model/magnetos/tsygan.html).

Protons acquire around $50keV$ as they drift toward the Earth from the Earth's magnetotail. These protons typically release the energies around $10keV$ into the ring current area under constant electric field $1mV/m$ when particles are close to the Earth. Ions spend around 30 minutes drifting to around $5R_E$ under the constant electric field $1mV/m$. Under a time-variable Gaussian electric field particles drift to the dusk side of the Earth and then float around to the noon area and drift back to the geomagnetic tail region. Particles release around $5 \sim 10keV$ into the ring current under a variable

electric field. The different electric models have quantitative differences in energetic gaining or losing. Under this cycle motion particles gain and release energy repeatedly until they intersect the Earth's ionosphere or escape away from the Earth.

Table of Contents

List of Tables

List of Figures

Chapter 1

Introduction

In this thesis I investigate how charged particles in the Earth's magnetosphere gain energy from the electric fields created by the solar wind blowing across the planet Earth and interacting with the Earth's internal magnetic field. A similar process occurs on all magnetized bodies in space. I devote a small part to the research on the same type of energizing processes that occurs on the Sun during the solar coronal mass ejections. The Sun is an important source of energetic protons and electrons.

Guiding center approximations are often described as "adiabatic" processes because the magnetic moment μ is nearly conserved before and after crossing the neutral sheet. The investigations based on a constant magnetic moment cannot explain the properties of behaviors in the neutral sheet.[*Swift*, 1977; *Gary* and *Lee*, 1982] In addition, the bounce motion invariant J is still nearly conserved in different action [*Speiser*, 1970; *Sonnerup*, 1971; *Whipple et al.*, 1986]. Some ions approach all the way to the edge of the sheet for the north-south bounce motion. *Kaufmann* and *Lu* [1993] referred to the orbits of these ions as "quasi-adiabatic". The ion orbits follow stochastic

orbits for some values of the geomagnetic orbit chaos index κ_{BZ} [*Chen* and *Palmadesso*, 1986]. These ions are generally called "non-adiabatic" because the magnetic moment μ has larger difference as particles intersect with the neutral sheet. On the other hand "non-adiabatic" means that ions gain or lose the energy and makes the particles behave in a more irregular nonlinear motion. We can utilize the Hamiltonian to define the transport coefficients to describe the properties of nonlinear phenomena [*Horton* and *Tajima*, 1990, 1991]. Ion motions with energies greater than $5keV$ cannot apply the guiding center approximations in the neutral sheet region. The Lorentz force equation is needed to describe most practical motions in the geotail due to the rapid change in the direction of $\mathbf{B}$ in crossing the equatorial plane [*Kaufmann et al.*,1993]. In contrast, electrons have small gyro-radius and are adiabatic up to energy of a few MeV.

Energy and momentum from the solar wind enter the tail region by way of the magnetopause. The magnetopause is the upper and lower boundary of the magnetosphere of the earth, which was first proposed by *Chapman* and *Ferraro* [1931]. The magnetopause separates solar wind plasma from terrestrial origin plasma. The current sheet lies in the center of the tail and separates the tail region from two lobes, the north and the south lobes. Each tail lobe connects to one of the polar caps. Figure 1.1 displays the configuration of the Earth's magnetosphere. We can estimate the radius of the geomagnetic tail by means of the magnetic flux conservation between the geotail lobe and

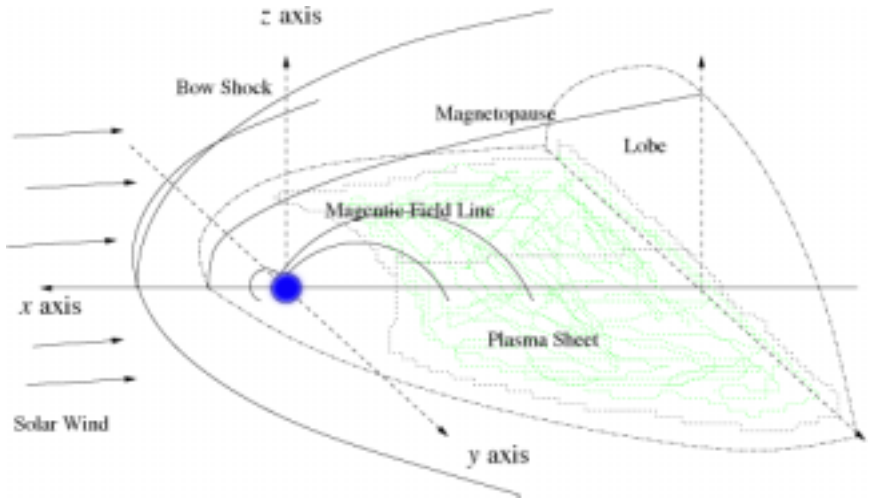

Figure 1.1: Simple configuration of the Earth's magnetosphere.

the polar cap $\Phi_{pc} = \Phi_{gt}$. The lobe flux $\Phi_{gt} \leq 10^9 wb$. The magnetic flux of the polar cup is $\Phi_{pc} = 2\pi(R_E \sin\theta_{pc})^2 B_\circ$; the magnetic flux of a tail lobe is $\Phi_t = \pi R_T^2 B_T/2$. The radius of the tail lobe is about $30R_E$ with colatitude angle between the equatorial plane and the polar cup 15°, the equatorial magnetic field $B_\circ$ 31,000nT at the surface of the Earth and the magnetotail field B_T 20nT. Here θ_{pc} is the time varying colatitude of the boundary of the polar cap (pc) which is at $\theta_{pc} \approx 25° \sim 30°$ (latitude 60° to 65°).

For a 50 percent charge of the tail flux in a 5 minute period the induced voltage is $\varepsilon = \triangle\Phi_{gt}/\triangle t = 160kV$. During geomagnetic substorms the geotail flux can nearly change by 5 percent. In the early 1960s the data observed from spacecraft documented the existence of the geomagnetic tail. These early spacecraft observations discovering the property of the geotail were reviewed

by *Ness* in 1987. Early measurements showed that the magnetic field strength of the near-Earth tail is around 20nT. The magnetic tail region is a reservoir of energy and during a substorm this stored energy is released violently.

The Lorentz force equation establishes the mechanism for the acceleration of the charged particle in the magnetosphere. The magnetic field does no work on the particles. Thus all charged particles acquire energy by drifting in regions with electric fields. I concentrate on the energy gained by the protons in this thesis. We can estimate how much energy the particle can obtain from the electric field. The voltage drops across the geomagnetic tail and ranges from $40kV$ in quiet times to $800kV$ within substorms. The energy gained by the protons can be greater than this potential by having sufficiently complex orbits. Particles carry and release the energy as drifting into the inner magnetosphere, *Van Allen* belts and the ionosphere. We study two models of electric fields and calculate the change of energy of typical protons. One of electric field models is the constant dawn-to-dusk electric field. The other one is that electric field is the function of time.

In Chapter 2 I discuss the properties of two coordinate systems we use and how to transfer from one coordinate system to the other one. One coordinate system is the Geocentric Solar Magnetosphere system (GSM). The other one is the Geocentric Solar-Ecliptic system (GSE). In Chapter 3 I use two magnetic field models to plot the magnetic configurations. The two mag-

netic models are Tsyganenko 96 model and Constant Current Model (CCM). In Chapter 4 I calculate by using the Lorentz force equation and guiding center approximations under no electric field working with Tsyganenko 96 model. And I compare the results from the Lorentz force with the ones from the guiding center approximations and look for the relationship between the magnetic moment μ with the chaos parameter κ_{BZ}. Then in Chapter 5 I simulate typical proton orbits with two types of electric field models to estimate the kinetic energy gained by the protons in moving from the deep geotail to the inner magnetosphere. Then I calculate some orbits on the process of the coronal mass ejection of the sun. Chapter 6 summarizes what I did in this thesis. Chapter 7 is an appendix and Chapter 8 is the references.

Chapter 2

Magnetic Coordinate Systems

2.1 Geocentric Solar Magnetospheric Coordinate System

The Geocentric Solar Magnetospheric coordinate (GSM) system is defined from the viewpoint of the earth. The x-axis of the GSM system is in the direction from the Earth toward the Sun. The Earth's magnetic dipole axis lies in the x-z plane. The positive z-axis is the same direction with the northern magnetic pole. The y-axis is chosen to be perpendicular to the earth's dipole in the dusk direction such that the coordinate system is right handed. The y-axis is always in the magnetic meridian. GSM longitude is measured from the x-axis to the y-axis in the xy plane. The GSM latitude is the normal direction from the xy plane to the positive z-axis. Figure 2.1 shows the configuration of the GSM system.

The GSM system is usually used to display the magnetotail magnetic fields because the geotail magnetic axis has the cylindrical symmetry formed by the solar-wind flow[21]. This system rotates toward the sun direction during a 365 days period because of the motion of the Earth around the Sun. To describe the path of the sun stretching over the sky, there is an another set

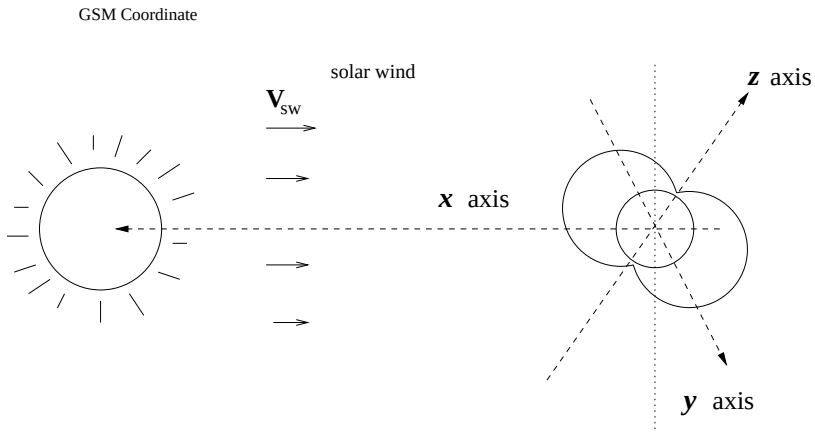

Figure 2.1: Geocentric solar Magnetospheric (GSM) coordinates. Two solid lines stand for the magnetic field configurations of the Earth. The vertical dotted line indicates the z axis of the GSE system.[4]

of spherical angles, solar zenith angle and solar azimuthal angle. The solar zenith angle is the angle of the Sun away from vertical at solar noon. The solar zenith angle is measured between the vector centered on the Earth and the x-axis of the GSM system. This solar zenith angle is the polar angle. The solar azimuthal angle is the angle measured from the projected vector in the yz plane of the GSM system. These angles would be used in raw data observed from satellites when doing "radio-metric corrections".

2.2 Geocentric Solar-Ecliptic Coordinate System

The Geocentric Solar-Ecliptic coordinate (GSE) system is from the viewpoint of the solar system. The definition of x-axis of GSE system co-

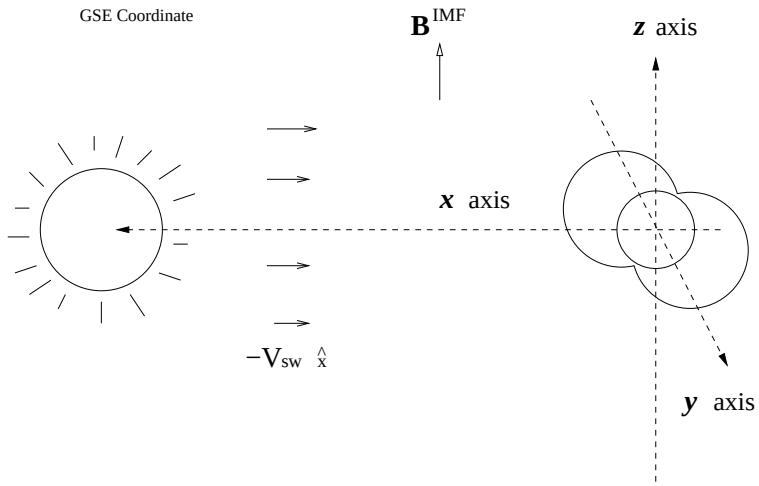

Figure 2.2: Geocentric solar ecliptic (GSE) coordinates. [4]

incides with GSM system. Its z-axis is pointing in the direction of the ecliptic pole. The y-axis is in the ecliptic plane directed to the dusk. The xy plane of GSE system is in the ecliptic plane. The longitude of GSE system is the angle measured from x-axis to y-axis in xy plane. And the latitude is the angle from xy plane to z-axis, positive for positive z-axis.

The GSE system is used to show the observed data of satellite, including solar-wind velocity, interplanetary magnetic field, and orbital motion. The GSE system is important in analyzing the solar-terrestrial relationship. Planetary motions in the solar system are described in the GSE system. Figure 2.2 shows the GSE system.

Hapgood[10] shows that the rotation angle transferring from GSE to

GSM can be calculated by a simple method given as follows. The magnetic dipole axis is projected on the GSE yz plane calibrated clockwise toward GSE z axis, which is an angle between the ecliptic dipole and the earth. This angle is the tilt angle ψ. It can be found as:

$$\psi = \cos^{-1}(\frac{Z_{\mathrm{GSM}}}{Z_{\mathrm{GSE}}}) \tag{2.1}$$

where ψ is between $+90^o$ and -90°. The GSM coordinates can be expressed by ψ and X_{GSE} as [24]:

$$\begin{aligned} X_{\mathrm{GSM}} &= \cos\psi X_{\mathrm{GSE}} + \sin\psi Z_{\mathrm{GSE}} \\ Y_{\mathrm{GSM}} &= Y_{\mathrm{GSE}} \\ Z_{\mathrm{GSM}} &= -\sin\psi X_{\mathrm{GSE}} + \cos\psi Z_{\mathrm{GSE}} \end{aligned} \tag{2.2}$$

This is the standard orthogonal rotation matrix $U(\psi)U^T(\psi) = 1$ about the y axis, where U(ψ) is written as follow:

$$U(\psi) = \begin{bmatrix} \cos\psi & 0 & \sin\psi \\ 0 & 1 & 0 \\ -\sin\psi & 0 & \cos\psi \end{bmatrix} \tag{2.3}$$

Each rotation could be expressed by two parameters: tilt angle ψ and the azimuthal angle θ, which is the angle between the vector $\mathbf{X}$(x, y, z) projected in the xy plane and y axis . The azimuthal angle θ here is defined as:

$$\theta = \tan^{-1}(\frac{y}{x}). \tag{2.4}$$

Properties, such as position, magnetic field vectors, in the GSE system could be transferred to GSM system through equation (2.2). The GSE and GSM coordinate systems are equivalent when the tilt angle is zero. For example the position (-10, 0, 0) R_E in GSE coordinate system can be transferred to (-9.17,

0 ,-3.99) R_E in GSM coordinate system with $\psi = 23.5°$ tilt angle. The origins of the GSE and GSM coordinates are the same (the center of the Earth).

All examples in this thesis use the GSM coordinate system. The Tsyganenko 96 model is also expressed in GSM system. Particle motions can be simulated through the Lorentz force equation or guiding center approximation after finding the magnetic field vector. The particles trajectories treated in section 5 are expressed by their components $\mathbf{r}(t) = (x, y, z)$ in the GSM system.

Chapter 3

Magnetic Field Models

According to Maxwell's equation $\nabla \cdot \mathbf{B} = 0$, which states mathematically that there is no magnetic mono-pole. The meaning of this condition is that $\mathbf{B}$ fields can not converge or diverge into a point. On the other hand, magnetic field lines are closed loops in space plasmas. From the mathematical formula $\nabla \cdot (\nabla \times \mathbf{F}) = 0$ for any differentiable vector $\mathbf{F}$, it is evident that one can introduce the idea of a magnetic vector potential ($\mathbf{A}$) as follows:

$$\mathbf{B} = \nabla \times \mathbf{A}. \tag{3.1}$$

Most magnetic models assume a magnetic vector potential $\mathbf{A}$ in the first step and use equation (3.1) to calculate the magnetic field.

The vector potential $\mathbf{A}$ and the magnetic field $\mathbf{B}$ are typically expressed in GSM coordinate for global problems. Simple magnetic field models are composed of four parts, (1) Earth's internal dipole field, (2) ring current field, (3) tail current field and (4) interplanetary magnetic field (IMF). Thus the mathematical formula that the model describes can be decomposed into four parts as: [18]

$$\mathbf{B}(\vec{x}) = \mathbf{B}_{dp}(\vec{x}) + \mathbf{B}_{rc}(\vec{x}) + \mathbf{B}_{t}(\vec{x}) + \mathbf{B}_{IMF}(\vec{x}). \tag{3.2}$$

The earth can be viewed as a giant magnet pointing southward. The magnetic dipole field comes from the currents in the molten core of the Earth. Field lines outside the earth are from the South connected to the North. The magnetic dipole moment has a tilt angle of about 11° relative to the Earth's North pole defined by the daily rotation. The magnetic moment $\mathbf{M_E}$ is about $8 \times 10^{15}\mathrm{T} \cdot \mathrm{m}^3$. If the core current is confined to within $r = R_E/5$, this implies a current of order $0.2\mathrm{GA}(2 \times 10^8\mathrm{A})$ with $\mathbf{M}$=BR^3 and $2\pi r\mathrm{B} = \mu_\circ \mathrm{I}$ for $r = R_E/5$. The charged particles near the earth are controlled by the magnetic dipole field instead of solar wind interaction.

Differential gradient and curvature drifts of electrons and ions produce the ring current. Positive ring current charges drift Westward in approximately circular orbits centered about the Earth in the inner magnetosphere between the range of $1.5R_E$ to $5R_E$. Ring current produces the southward directed field $\mathbf{B_{rc}}$ inside the ring and decreases the strength of the surface magnetic field at low latitudes. The fluctuations of the southward surface magnetic field component is a direct measure of the net ion energy contained in the ring current. In addition, the partial-ring current also floats partway around the earth in the middle magnetosphere. [21] This partial current is also called the Birkeland current. The partial ring current links the geotail and magnetopause boundary layer. The strength of the ring current is controlled by the solar conditions. An Eastward electrical field, corresponding to a southward interplanetary magnetic field, can be significant to the ring current and the

D_{st} index. The D_{st} index stands for the world magnetic storm level. The D_{st} index is calculated by averaging the horizontal component of magnetic field for the mid-latitude and equatorial magnetograms all over the world. Negative value means a magnetic storm is in progress. Stronger magnetic storms cause the more negative value of D_{st} index. A strong storm like the Bastille day storm of July 14, 2000, produced a D_{st} of -300nT(www.gsfc.nasa.gov).

The geotail region is the part of the magnetosphere on the opposite side of the Sun that extends from about $10R_E$ to $100R_E$. Modeling the tail current by infinitely thin sheet or by finite thickness with discontinuous volume current density are difficult to do mathematical calculations[23]. The geotail comes from the interaction between the magnetized solar wind plasma and the geomagnetic field [18]. This region is a large reservoir of the plasma and magnetic energy. The energy and plasma are injected into the inner magnetosphere without a fixed period from the geotail region. Strong periods are called injection events and are associated with substorms. The plasma current sheet is in the center of the tail and contains approximately 20MA of current that flows parallel to ring current. There are two lobes (south and north) separated by current sheet . The magnetic fields of two lobes are the direction toward the Earth in the north lobe and away from in the south lobe. Hence a large current plasma separates the oppositely directed magnetic field.

The width size of the static geotail is caused by the balance between

the pressure of the solar wind and that of the plasma sheet pressure. The tail current for static current can be found by applying Ampere's law $\nabla \times \mathbf{B} = \mu_\circ \mathbf{J}$. Assuming the average radius of lobe is $10R_E$. The lobe volume Ω_{lobe} is around $100R_E(\pi(10_{RE})^2) \approx 10^{25}m^3$. For the solar wind pressure of 5 nPa associated with $B^2/2\mu_o$, the magnetic energy W_m is equal to $\int (B^2/2\mu_o)dV \approx P\Omega_{lobe}$ around $5 \times 10^{16}J$. In a substorm the pressure may drop to 1 nPa releasing $10^{16}J$ in 20 minutes. The associated power is $8.3 \times 10^{12}W(Watts)$. This surge of $8.3 \times 10^{12}W$ energizes particles and produces the auroral brightening of the ionosphere.

The Sun's magnetic field is Interplanetary Magnetic Field (IMF). The direction of IMF can be directed to any direction because the Sun rotates once about 27 days. The solar wind brings the sun's magnetic field through the whole solar system. The solar wind in interplanetary space has a spiral geometry at some heliocentric distance where field lines are open and radial. The IMF and the earth's magnetic field connect at the magnetopause. If the IMF points to the south, it cancels partially the earth's magnetic field. The field lines from the south pole readily connect to the southward IMF. The particles of solar wind can reach the atmosphere of the earth and put energy into the magnetosphere.

3.1 Tsyganenko 96 Model

N. A. Tsyganenko and his collaborators developed a series of magnetic fields in the 1980's. [Tsyganenko, 1982 [29]; Tsyganenko, 1987 [24]; Tsyganenko 1989 [25]] Model 96 was released on June 22, 1996. The models are simple physical parameterizations of the plasma currents with the parameters determined by satellite measurements of the magnetic field. The Tsyganenko 96 model is described in GSM coordinates. It is controlled by the pressure of the solar wind, Disturbance short-time index (D_{st}) and the direction and magnitude of the interplanetary field (IMF). The Tsyganenko 96 model does not use Planetary magnetic activity (K_p) as a parameter. Tsyganenko 96 model is composed of ring current, tail current and region 1 and 2 Birkeland current systems. All currents are within the magnetopause. Tsyganenko employed the method proposed by Schulz and McNab (1987), which used shielding potentials to build the Earth's dipole, ring current and the cross-tail current sheet. The magnetic field can reduce to a simple superposition problem. The magnetic field is a sum of model 96 and Earth's magnetic dipole field. The size of the magnetopause in this model is determined by the pressure of the solar wind which is a dynamic pressure $P_{sw} = \rho_{sw} v_{sw}^2$ from the supersonic flow speed $v_{sw} \gg (k_B T_{sw}/m_p)^{1/2}$, where ρ_{sw} is the mass density of solar wind and v_{sw} is the solar wind velocity. Parameters of the Tsyganenko 96 model should range within the following intervals for a reliable calculation:

1. Pressure of the solar wind between 0.5 and 10 nPa.

2. D_{st} between -100 and +20 nT.

3. B_y^{IMF} and B_z^{IMF} both between -100 and 10 nT.

The ring current is approximately axially symmetric under a cylindrical coordinate system (ρ, φ, z). Region 1 and Region 2 Birkeland current systems can contribute partially to the ring current. The currents have an extent in z direction. The magnetic vector potential $\mathbf{A}$=$A(\rho, z)\tilde{\varphi}$ can be written assuming $\nabla \times \nabla \times \mathbf{A} = 0$ outside the current sheet ($z \neq 0$) as: [24]

$$\frac{\partial}{\partial \rho}(\frac{1}{\rho}\frac{\partial}{\partial \rho}(\rho A)) + \frac{\partial^2 A}{\partial z^2} = 0 \tag{3.3}$$

The general solution of this partial differential equation $A_\varphi = A$ is: [25]

$$A(\rho, z) = \int_0^\infty \lambda^{1/2} C(\lambda) J_1(\lambda\rho) \exp(-\lambda|z|) d\lambda \tag{3.4}$$

where J_1 is the first order Bessel function. $C(\lambda)$ is the distribution function of currents in current sheet and determined from the boundary condition. The magnetic vector potential leads to a feasible expression of the magnetic field at the boundary of the current sheet as:

$$B_z(\rho) = \frac{1}{\rho}\frac{\partial(\rho A)}{\partial \rho}|_{z=0} \tag{3.5}$$

Taking (3.4) into (3.5), the magnetic field $B_z(\rho)$:

$$B_z(\rho) = \rho^{-1/2} \int_0^\infty \lambda C(\lambda) J_o(\lambda\rho)(\lambda\rho)^{1/2} d\lambda \tag{3.6}$$

Inverting the transformation (3.6), we arrive at:

$$\lambda C(\lambda) = \int_0^\infty \rho^{(-1/2)} B_z(\rho)(\lambda\rho)^{1/2} J_o(\lambda\rho) d\rho.$$

In order to employ the satellite data, Tsyganenko applied least square fitting to an experimental data set. The magnetic field is restricted to distribution $B_z(\rho)$. The analytical forms of magnetic vector potential are connected with expression for $A(\rho, z)$. The most appropriate solution corresponding to distribution B_z is:

$$B_z(\rho) \sim (a^2 + \rho^2)^{-1/2}. \tag{3.7}$$

It provides maximum distribution at the center ($\rho = 0$) and the zero distribution when $\rho \to \infty$. The corresponding magnetic vector potential is expressed: [Bateman and Erdelyi, 1954]

$$A(\rho, z) \sim \rho^{-1}\{[(a + |z|)^2 + \rho^2]^{1/2} - (a + |z|)\}. \tag{3.8}$$

Taking the first and second derivatives:

$$A^{(1)}(\rho, z) = \frac{\partial A}{\partial a} \sim \rho^{-1}\{1 - \frac{a + |z|}{[(a + |z|)^2 + \rho^2]^{1/2}}\} \tag{3.9}$$

$$A^{(2)}(\rho, z) = \frac{\partial A^{(1)}}{\partial a} \sim \rho[(a + |z|)^2 + \rho^2]^{-3/2} \tag{3.10}$$

Only (3.10) can produce the current distribution $I(\rho)$ with a finite magnetic moment

$$M = \frac{\pi}{c} \int_0^\infty I(\rho)\rho^2 d\rho. \tag{3.11}$$

Equation (3.10) is also similar to the vector potential of a ring current model Tsyganenko proposed in 1982 [29].

Two models of the magnetotail current can approximate a realistic magnetotail more closely than one global formulation. The tail currents of Tsyganenko 96 model includes two models; one is for the near-Earth tail current. The other one is for the tail field of the far magnetotail. Tsyganenko [26] adopted many approximations to describe the two-dimensional warping with tilt angle in which coefficients of tail currents are determined by spacecraft magnetometers data because there is not enough information about how the earth's dipole tilt influence the tail current sheet. The return current of the central tail current sheet can be found across the lobes and magnetopause. The return current can be divided into two parts, symmetrical and anti-symmetrical with respect to the dipole tilt ψ. The first is the main field with respect to the perpendicular dipole field of the Earth. The anti-symmetrical part is between the northern and southern lobes rising. The rest of the tail field in the far magnetotail is provided by the Chapman-Ferraro current because there is no current outside the magnetopause. The near-Earth tail current comes from the region 1 and 2 Birkeland current systems. [27] Therefore, the net cross-tail field can be expressed as:

$$\mathbf{B}_{CT} = \alpha_{T1}\mathbf{B}_{CT1} + \alpha_{T2}\mathbf{B}_{CT2} + \alpha_{T3}\mathbf{B}_{CT3} \tag{3.12}$$

where α_{T1}, α_{T2} and α_{T3} are the weight factors of far-tail current, Region 1 and Region 2 Birkeland currents respectively.

3.2 Constant Current Model

Using a two-dimensional model has many advantageous properties. The 2D approximation is valid for $|y| < 10R_E$ and $|z| < 10R_E$ in the central plasma sheet. Two-dimensional models of the magnetosphere qualitatively reproduce many of the truly three-dimensional magnetosphere, though quantitatively they can be in serious error. The Constant Current Model (CCM) is a two-dimensional magnetic field model written in GSM coordinates. It is a simple model of the current sheet. The CCM discuss the local stability of a dipolar magnetic plasma equilibrium[7]. The fundamental idea of the CCM model is to assume force balance:

$$\nabla P = \mathbf{J} \times \mathbf{B} \tag{3.13}$$

where P is an isotropic pressure. The CCM Model is defined in the $x - z$ plane. Thus selecting $\mathbf{A}$=$A_y\hat{\mathbf{e_y}}$ implies $\mathbf{J}$=$J_y\hat{\mathbf{e_y}}$. Through Ampere's law, the J would be written as:

$$\mathbf{J} = J_y\hat{\mathbf{e_y}} = \frac{1}{\mu_o}\nabla \times \mathbf{B} = -\frac{1}{\mu_o}\nabla^2 A_y\hat{\mathbf{e_y}} \tag{3.14}$$

where we use

$$\mathbf{B} = \nabla \times (A_y\hat{\mathbf{e_y}}) = \nabla A_y \times \hat{\mathbf{e_y}} \tag{3.15}$$

from equation (1). If the pressure $\mathbf{P}$ is the function of A_y, it satisfies with:

$$\frac{dP}{dA_y} = -J_y, \tag{3.16}$$

since $\nabla P = (\partial P/\partial A_y)\nabla A_y$ and $\nabla P = \mathbf{J} \times \mathbf{B} = J\tilde{\mathbf{e}}_{\mathbf{y}} \times \mathbf{B} = -JB\nabla A_y$. The magnetic flux function ψ is equal $-A_y$. On the other hand, the pressure gradient at x, z is equal to current sheet and current density at x, z. The pressure gradient is a constant along the Magnetic field line because $\mathbf{B} \cdot \nabla P = 0$ when $\mathbf{P} = P(A_y)$. Thus pressure is the linear function of $\psi = -A_y$ in the Constant Current Model [8].

The model is obtained from the sum of quadratic vector potential and a two-dimensional dipole field as follows:

$$A_y(x, z) = -\frac{B_o r_o^2 x}{x^2 + z^2} - \frac{1}{2}B'_x z^2 + B_n x \tag{3.17}$$

where $B_o r_o^2$ is the magnitude of two-dimensional magnetic dipole, B_n is due to external currents and B'_x is the uniform central plasma sheet current as a consequence of the diamagnetic current (j_y), which is proportional to current. Furthermore, B_n is a northward uniform field correlated with the IMF B_z [6]. In GSM coordinate $x < 0$ is the nightside region. The x and z field components are given as:

$$B_x(x, z) = B'_x z - \frac{2B_o r_o^2 xz}{(x^2 + z^2)^2} \tag{3.18}$$

$$B_z(x, z) = B_n + \frac{B_o r_o^2 (x^2 - z^2)}{(x^2 + z^2)^2} \tag{3.19}$$

Equation (3.18) and (3.19) are the mathematical formulas of the Constant Current Model. One easily verifies that $\nabla \cdot \mathbf{B} = 0$ and $\nabla \times \mathbf{B} = B'_x \hat{y}$. Figure

3.1 shows the field lines of the two models: the upper panel is computed with the Tsyganenko 96 model; the bottom is computed with the Constant Current Model. Constant Current Model can be similar to Tsyganenko 96 model by finding appropriate parameters through model fitting.

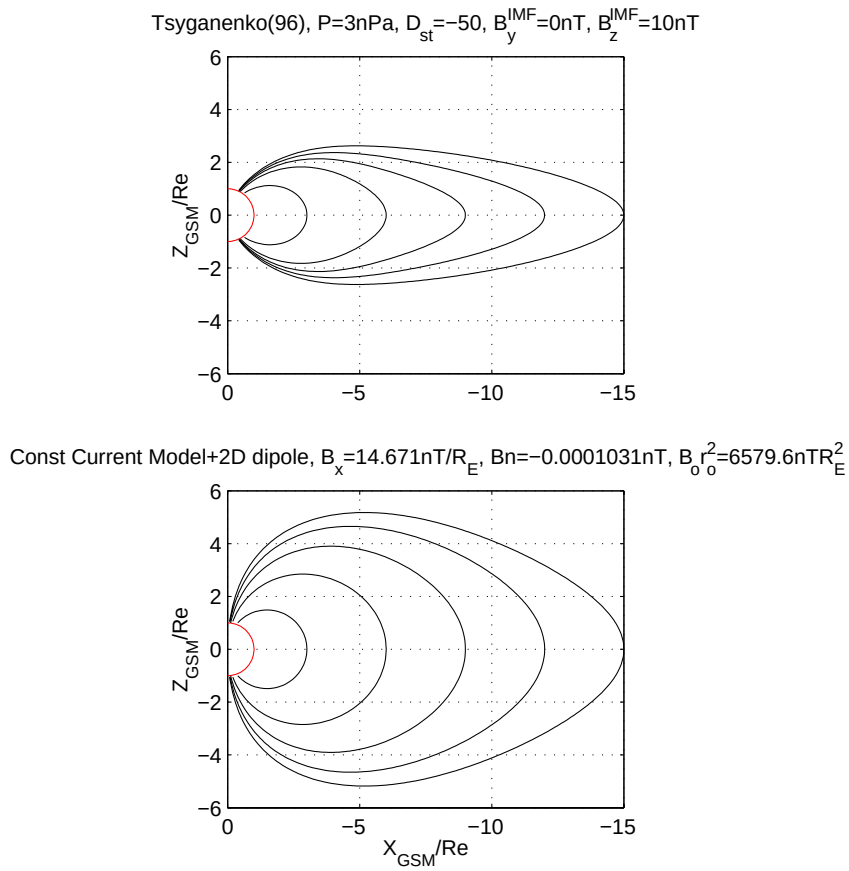

Figure 3.1: Magnetic field lines of two models; upper one is Tsyganenko 96 Model, where P_{dyn}=3.0nPa, D_{st}=-50nT, B_y^{IMF}=0.0nT and B_z^{IMF}=10.0nT. The bottom plot is 2-D Constant Current Model, where B'_x=14.671.0nTR_E^2, B_n=-0.0001031nT and $B_o r_o^2$=6579.6 nT$(R_E)^2$.

Chapter 4

Charged Particle Motion in the Geotail

4.1 Equations of Motion

The Lorentz force determines the equations of motion of charged particles in the magnetosphere. The motion of charged particles can be given as a superposition of rotation perpendicular to the magnetic field, motion parallel to the magnetic field and drift. The idea, which is rotation perpendicular and parallel to the magnetic field, develops the guiding center approximations. The guiding center approximations is the average of the full orbits. The motion parallel to the magnetic field can be understood in terms of adiabatic invariants. The electromagnetic properties of the geotail are given and the numerical results of practical motion are compared to the theoretical treatment.

Charged particles follow the equations of motion to drift and accelerate in the magnetosphere. Locally the particle can be seen as moving in an almost homogeneous field. Thus the radius of particle gyro-motion for a single turn is typically fairly small. Particle motions are constrained according to the conservation laws, including the conservation of mass, energy and charge [1]. In addition, there are approximate invariants called the first and second

adiabatic invariants that partly constrain the motion of the charges.

4.2 Geotail

Geotail region is typically the geomagnetic tail which is the region far behind the earth's magnetosphere. Momentum and particles could enter the tail region across the magnetopause. The geomagnetic tail behaves as a reservoir of plasma and magnetic energy. A current sheet lies in the center of the tail. The two lobes (North and South) are divided by a high pressure plasma current sheet. In a static tail the geometry of the distant tail is determined by the pressure balance between the tail lobes and the solar wind pressure. From the data observed from $IMP6$ the distances of the magnetotail is around $30R_E$. The direction of magnetic field in the north lobe is toward the earth. But in the south lobe the direction of magnetic field is away from the earth.

The early measurements gave that the strength of the near-earth geomagnetic tail is about 20nT. This value is large compared to what the dipole field would be at this location. Through Ampere's law the relationship between the magnetic field and sheet current density can be derived as $2B = \mu_\circ I/L_x$. This relationship gives around $I/L_x = 30mA/m$ when magnetic field is around 20nT. Equivalently the tail can carry $2 \times 10^5 A \cdot R_E^{-1}$.

4.3 Lorentz Force Orbits

The Lorentz force law can describe the influence of a charged particle moving in electric and magnetic fields. Electrical and magnetic forces are essential to understand the behaviors of particles because plasma is a quasi-neutral electrically conducting gas. Consider a charged particle q with the velocity $\mathbf{v}$ and an electrical field $\mathbf{E}$ and a magnetic field $\mathbf{B}$. The particle experiences the force $\mathbf{F}_L$, which is the Lorentz force:

$$\mathbf{F}_L = q(\mathbf{E} + \mathbf{v} \times \mathbf{B}). \tag{4.1}$$

The magnetic field acts on particles only in the direction perpendicular to the particle motion because of $\mathbf{v} \times \mathbf{B}$. A charged particle moves in a circle in the uniform magnetic field with $\mathbf{E}$=0. The angular frequency can be found through force equilibrium as:

$$\Omega_c = \frac{qB}{m}, \tag{4.2}$$

where Ω_c is also called gyro-frequency or cyclotron frequency. The radius r_L of the gyro-orbit is determined by the velocity component $v_\perp$ perpendicular to the magnetic field. The radius is expressed as [2]:

$$\mathbf{r}_L = \frac{\mathbf{v} \times \mathbf{B}}{\Omega_c B}. \tag{4.3}$$

The magnitude of (4.3) is generally called the Larmor radius:

$$r_L = \frac{v_\perp}{\Omega_c} = \frac{m v_\perp}{qB} \tag{4.4}$$

Taking the scalar product of (4.1) by velocity $\mathbf{v}$ to derive the rate of increase of the kinetic energy

$$\frac{d}{dt}(\frac{1}{2}mv^2) = q\mathbf{v} \cdot \mathbf{E}. \tag{4.5}$$

Since the orbits are very complicated the time integral of the right-hand side of equation (4.5) is not well known. This equation shows that the magnetic field does no direct work on the particle because the magnetic field does not change the kinetic energy. However, the magnetic field strongly influences the orbit and thus modifies velocity and position so that the power $q\mathbf{v} \cdot \mathbf{E}$ is strongly influenced by the magnetic field.

4.4 Guiding Center Orbits

The guiding center is the average position of a turn when a particle moves during this short time of $2\pi/\Omega_c$. The guiding center slides along the direction of magnetic field. The guiding center can be defined as the vector sum of position $\mathbf{r}$ and Larmor radius $\mathbf{r}_L$:

$$\mathbf{r}_{gc} = \mathbf{r} + \mathbf{r}_L = \mathbf{r} + \frac{\mathbf{v} \times \mathbf{B}}{\Omega_c B}. \tag{4.6}$$

Particles spiral around the guiding center. Guiding center orbits are analyzed by cyclotron motion from the slow drift averaged particle location.

Orbits can be described as three parts, gyration around the magnetic field line, bounce back and forth along the field line between reflection points,

which is often called mirror points and diamagnetic drift around the earth. In general, drift velocity can be simply expressed:

$$\mathbf{v}_{gc} = \mathbf{v}_{\parallel} + \mathbf{v}_{\perp}. \tag{4.7}$$

It is straightforward to verify that $d\mathbf{r_{gc}}/dt = v_{\parallel}\hat{\mathbf{b}} + \mathbf{V_F}$ when $\mathbf{B}$=constant by taking the derivative of equation (4.6) and using equation (4.1) for $md\mathbf{v}/dt = \mathbf{F_L}$. $\hat{\mathbf{b}} = \mathbf{B}/B$ is the direction along the magnetic field line.

Force items, such as electric field, gravity and gradient magnetic field, can give the guiding center a drift velocity transverse to the magnetic field. Using the Lorentz force can express any transverse force $\mathbf{F}_{\perp}$ acting on a gyrating particle in magnetic field and give a drift perpendicular to both $\mathbf{F}_{\perp}$ and $\mathbf{B}$:

$$\mathbf{v}_F = \frac{\mathbf{F}_{\perp} \times \mathbf{B}}{qB^2}. \tag{4.8}$$

Through the guiding center theory, the drift velocity can be decomposed into four parts: (1) velocity parallel to field line, (2) $\mathbf{E} \times \mathbf{B}$ drift, (3) curvature drift and (4) gradient B drift. The formula of drift velocity can be written as:

$$\mathbf{v}_{gc} = v_{\parallel}\hat{\mathbf{b}} + \frac{\mathbf{E} \times \mathbf{B}}{B^2} + \frac{mv_{\perp}^2}{2qB^3}(\mathbf{B} \times \nabla B) + \frac{mv_{\parallel}^2}{qB^2}(\mathbf{B} \times \boldsymbol{\kappa}), \tag{4.9}$$

where $\hat{\mathbf{b}}$ is the unit vector $\mathbf{B}$/B; and curvature vector $\boldsymbol{\kappa} = (\hat{\mathbf{b}} \cdot \nabla)\hat{\mathbf{b}}$. The second term of the right hand side of equation (4.9) is the $\mathbf{E} \times \mathbf{B}$ drift. This drift is independent of particle mass, charge and energy. Thus, the drift direction

of the ion is the same with the electron. The third term of the right hand side of equation (4.9) is called the gradient B (or ∇B) drift. In an inhomogeneous magnetic field, the direction of gradient magnetic field is perpendicular to $\mathbf{B}$ and causes a drift transverse to magnetic field. The direction of the ∇B drift depends on the sign of charge q of the particles. Because electrons drift opposite to ions, the drifts produce a substantial electrical current perpendicular to magnetic field. The fourth term of equation (4.9) in the right hand side is curvature drift. If the configuration of magnetic field is not a straight line, particles experience a centrifugal force in following the curved magnetic field lines. The centrifugal force increases radius of gyration; the particle thus drifts again in the direction perpendicular to the magnetic field [21]. These two drifts do not influence each other.

Guiding center particles are often viewed as "adiabatic" because the magnetic moment μ (first adiabatic invariant) is close to invariant [17]. The magnetic moment is

$$\mu = \frac{W_\perp}{B} = \frac{mv_\perp^2}{2B}. \tag{4.10}$$

Adiabatic invariant means the parameters of system, such as the field strength, change slowly, then the action changes much less than the field geometry.[9] The magnetic moment μ is based on Lorentz force equations. The magnetic moment μ can play an important role in constraining the high-energy electrons in cyclotron resonance or magneto-discharges. Particles are affected by the

force parallel to the magnetic field and can be expressed to

$$m\frac{dv_{\parallel}}{dt} = -\mu\frac{\partial B}{\partial s}. \tag{4.11}$$

For each energy E and magnetic moment μ the particle reaches the mirroring point a and b when the position s is such that $E = \mu B(s)$. This defines $S_a(\mu/E)$ and $S_b(\mu/E)$. Equation (4.11) multiplied by $v_{\parallel}$ can obtain the equation of energy conservation

$$\frac{d}{dt}(\frac{mv_{\parallel}^2}{2}) = -\mu\frac{\partial B}{\partial s}\frac{ds}{dt} = -\mu\frac{dB}{dt}. \tag{4.12}$$

Under adiabatic condition $dE/dt = 0$ we can express as

$$\frac{d}{dt}(\frac{mv_{\perp}^2}{2} + \frac{mv_{\parallel}^2}{2}) = \frac{d}{dt}(\frac{mv_{\parallel}^2}{2} + \mu B) = 0. \tag{4.13}$$

Substituting equation (4.12) into (4.13) can get

$$-\mu\frac{dB}{dt} + \frac{d}{dt}(\mu B) = 0 \tag{4.14}$$

and be reduced to

$$\frac{d\mu}{dt} = 0. \tag{4.15}$$

The magnetic moment conservation implies the particles possess the higher perpendicular velocity as particles drift to the higher strength region of magnetic field. Since the energy of particle is constant, $v_{\parallel}$ decreases as $v_{\perp}$ increases. We show an example orbit with $\triangle\mu/\mu \ll 1$ below.

When guiding center parallel motion is periodic, such as mirror motion, there exists what is called the "second adiabatic invariant" given by:

$$J = \oint_a^b p_{\|} \cdot ds. \tag{4.16}$$

The symbol $\oint$ indicates the integral is taken as though the orbit were periodic. A trapped particle bounces within mirror points a and b. The true orbits are the spiral motions drifting along the magnetic field lines. However, orbits can be viewed as effective point particles moving with $\mathbf{r_{gc}}(t)$ orbits to compute the equation (4.16) under guiding center approximation. The J is conserved as long as the particle experiences the magnetic field variation on time scale longer than bounce period $\tau(a, b)$. For the nearly periodic cyclotron orbits the action integral $\mathrm{I} = \oint_a^b \mathbf{p}_\perp \cdot \mathbf{dr}_\perp$ is proportional to the magnetic moment μ, which is described as:[11]

$$\mathrm{I} = \frac{2\pi\mu m}{q}, \tag{4.17}$$

where m and q are the mass and charge respectively. Here, the magnetic moment is $\mu = mv_\perp^2/2B$. Particles can drift for a long distance as long as μ and J have the same value.

An example of this is from *McIlwain* in 1961[19]. *McIlwain* mentioned that the magnitude of the magnetic field $\mathbf{B}$ and the integral invariant I_{mc} had been found to measure at different geographic places. The integral invariant at location a is defined as:

$$I_{mc} = \oint_a^{a'} (1 - B(s)/B)^{1/2} ds \tag{4.18}$$

where ds is the length along the magnetic field line between point a and a', $B(s)$ is the magnetic field along the magnetic field line, B is the magnetic field of the point a. Under no electric field the I_{mc} is defined as

$$I = P^{-1} \oint_{a}^{a'} P_{\|} ds \tag{4.19}$$

where $P_{\|}$ is the parallel momentum along the magnetic field line, and P is the total momentum at the location a. The magnitude of the force perpendicular to the field line has the same B and I if the energy and mirror point distributions of trapped particles do not change significantly during the period the slowest particle drifts around the earth.[19]

Figure 4.1A shows the value of J at the equatorial plane in the nightside region for a given $E_\circ$ and μ values. We use $J \rightarrow J/\sqrt{2mE_\circ}$ where $\lambda = \mu B_{min}/E_\circ$ with $\mathrm{B_{min}} = \mathrm{B(x, y, 0)}$. In figure 4.1A we use $\lambda = 0.1$. The darker area means that the figures of J are bigger over there. It means a particle can drift a longer distance. Since J is constant the guiding center must drift on the closed contours J=constant in figure 4.1A. For $x \sim -10R_E$ the guiding center orbit is trapped in the tail circles for $x > -7R_E$ the guiding center drifts around the Earth. Figure 4.1B indicates the longest distance particles can drift in the northern hemisphere. The unit of distance is in the earth radius R_E. Because J is conserved, as well as μ, the particle must bounce at the same altitude when it drifts around the earth. At point (-15,0) the J and distance S are 3.20 $km/s \cdot R_E$ and $5.1R_E$ respectively; at point (-7,0) the J is

2.52 $km/s \cdot R_E$ and S is $3.4R_E$. Particles can drift the longer length if J is large.

We use figure 4.1A and 4.1B to estimate the average parallel velocity of an orbit by taking the ratio J/S. At the point (-15,0) we can get $< v_{\|} >=$ $3.2km/5.1s= 0.63km/s$ and at point (-7,0) we obtain $< v_{\|} >= 2.52km/3.4s=$ $0.74km/s$.

The conservation of magnetic moment μ indicate that a varying magnetic field heats or cools a plasma according to equation (4.14) and equation (4.15). The conservation of J can be applied to define a coordinate system which is appropriate to map distributions of geomagnetically trapped particles [1]. The importance of μ and J adiabatic conservation is that it applies under general conditions for asymmetric fields and in the presence of (weak) electric fields.

4.5 Adiabatic compared with Exact Orbits

Both Lorentz force equation and guiding center theory can be used to simulate the particle orbits in the geotail. A proton possesses $1keV$ initial energy as drifting in the geotail in figure 4.2, figure 4.3 and figure 4.4. Figure 4.2 shows the complete gyration orbit calculated by Lorentz equations under no electric field when a particle drifts for 100 seconds. Here the Tsyganenko 96 model as the background magnetic field. The parameters of the Tsyganenko

Initial Position(x, y, z)	(-10, 0, 0) R_E
Pitch Angle ψ	60°
Gyrophase Angle θ	60°
Initial Energy	$1keV$
Initial Velocity	$438kms^{-1}$
Velocity Components(v_x, v_y, v_z)	(328.53, 189.68, 219.02) km/s
Initial Magnetic Moment μ	$0.44keV$/nT

Table 4.1: The initial conditions of the particle in figures

96 model are: P_{dyn} = 3nPa, $D_{st} = -50$nT, B_y^{IMF} = 0nT and B_z^{IMF} = 10nT. The equatorial pitch angle ψ, which is the angle between z-axis and velocity vector, is 60° and the gyrophase angle θ is 60° where the angle is measured between the projection of the particle initial velocity $\mathbf{v}$ to equatorial plane and y-axis. The viewpoint of the figure 4.2 is in three dimensions for this proton $\mu = 0.044keV$/nT. Figure 4.3 decomposes figure 4.2 into two dimensions. Figure 4.3A is in midnight meridian; Figure 4.3B is in equatorial plane. By using guiding center theory there is the displacement in y direction under no electric field, shown in figure 4.4. It implies that the curvature drift and ∇B drift have a force transverse to the field line and cause this displacement. The detail of the initial conditions are shown in table 4.1.

The assumption of guiding center theory is parameters of the system $X(t)$, such as the field strength B, change slowly as described by:[9]

$$\frac{1}{\tau} \gg \frac{1}{X}\frac{dX}{dt} \tag{4.20}$$

where X is any field quantity and τ is the oscillation period. In the figure

4.6C the magnetic moment μ changes from around 0.07 to 0.25 at 232 second. According to equation (4.20) $1/\tau$ is $1/232 \approx 0.004$ and change of the magnetic moment $\triangle\mu/\triangle t$ products $1/\mu$ is around 0.36. These numbers do not correspond to the equation (4.20) and the assumption of guiding center does not work. The magnetic moment μ is not conserved because of the significant field changes on the length scale of their Larmor radius[5]. Figure 4.5 indicated the guiding center calculated from equation (4.6) is almost similar to the result from guiding center theory in 100 seconds.

Guiding center approximations can not be used to describe the ion motions in neutral sheet region if a particle drifts for a long time [18]. Suppose three protons possess different initial energy $0.1keV$, $1keV$ and $10keV$ with the same gyrophase angle $\theta = 60°$ and pitch angle $\psi = 60°$. Figure 4.6 shows the magnetic moment versus time with different initial energy, $0.1keV$ in figure 4.6A, $1keV$ in figure 6B and $10keV$ in figure 6C respectively. The unit of the magnetic moment μ is keV/nT. There is no energy loss or gain during the drifting period. In figure 6A the magnetic moment μ is almost constant before or after the neutral sheet. However there are small perturbations in figure 6B when the initial energy increases to $1keV$. In figure 6C the magnetic moment μ has intense variation. Thus the magnetic moment μ responds sharply and is not the constant as crossing the neutral sheet with the energy increasing. The guiding center approximations can describe the properties of the particle before the period crossing the neutral sheet and after the crossing. There are

some limitations for using guiding center theory.

The probability distribution $P(\mu)d\mu$ with the low initial proton energy is similar to Gaussian distribution function, shown in figure 4.7. Initial proton energy are $1keV$ and $10keV$ in figure 4.8 and in figure 4.9 respectively. With the increasing energy the standard deviation increases and the distribution function is not similar to Gaussian distribution function. Non-Gaussian distribution stands for that particles are energized. Thus the magnetic moment is not adiabatic as distribution function is non-Gaussian distribution because particles are energized.

We can also discuss the relationship between chaos parameter and magnetic moment μ. The definition of chaos parameter is[13]

$$\kappa_{BZ} = (\frac{R_c}{\rho})^{1/2}, \tag{4.21}$$

where ρ is Larmor radius and R_c is curvature radius. All chaos parameters in cases we mentioned are larger than 2. In general $\kappa_{BZ} \geq 2$ the magnetic moment $\mu = mv_\perp^2/2B$ is a good adiabatic invariant. Under low initial proton energy the magnetic moment μ varies slightly and the chaos parameter corresponding to the magnetic moment μ looks like a periodic function. As a particle crosses the neutral sheet the magnetic moment μ pulsates. However the chaos parameter is lower at the position where the particle crosses the neutral sheet. As increasing proton energy the chaos parameter versus time does

not look like the periodic moment. The chaos parameter is lower when a particle crosses the neutral sheet. Figure 4.10, 4.11 and 4.12 show the relationship between the magnetic moment μ and the chaos parameter κ_{BZ} with different energy. There are larger chaos parameter κ_{BZ} as smaller magnetic moment μ. The step-like changes in μ shown in figure 4.12 suggests that the standard map in chapter 4 of $Horton$ and $Ichikawa$[13] can be used to decide the change of μ.

The standard map can be employed to measure the change of the magnetic moment μ. For appropriate dimensionless parameters are easily $X \rightarrow kx/2\pi$, $P \rightarrow kp/m_{\circ}\omega$ and $T \rightarrow \omega t$. P is the particle momentum perpendicular to the field line of the force and X is the location of the particle. $Horton$ defined a parameter for relativistic standard map so that[13]

$$K = \triangle\mu \tag{4.22}$$

is the jump in the magnetic moment when the particle crosses the equatorial plane. The motion gives the map

$$\mu_{t+1} = \mu_t - \frac{K}{2\pi} sin(2\pi\theta_t) \tag{4.23}$$

$$\theta_{t+1} = \theta_t + \mu_{t+1}. \tag{4.24}$$

Here t stands for the time sequence of the particle crossing the equatorial plane. The reference of the map is seen clearly in figure 4.6 and 4.12 when the $10keV$ proton makes a jump in μ everytime it crosses the equatorial plane.

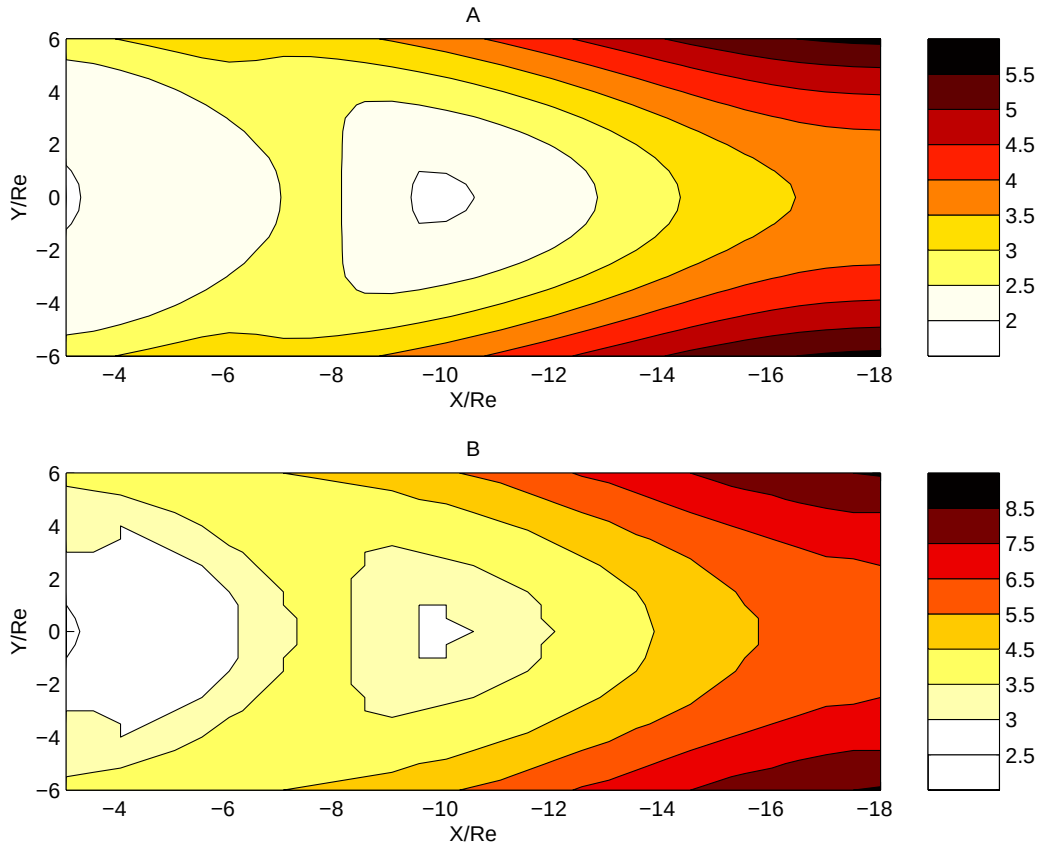

Figure 4.1: Parameters of Tsyganenko 96 model: P_{dyn}=3.0nPa, D_{st}=-50nT, B_y^{IMF}=0.0nT and B_z^{IMF}=-10.0nT. The top figure (A) is contours of constant values of the second adiabatic invariant $J = \int \sqrt{1 - \lambda B(s)/B_\circ} ds$ from equation (4.16), where λ is pitch angle variable $\mu B_\circ / E_\circ$. The value of λ is 0.1. $B_\circ$ and $E_\circ$ are magnetic field and energy at initial position respectively. The bottom (B) is contour of the magnitude of distance S=S(x, y, z=0) particle drifts, which is computed from $S = \int_a^b dS$.

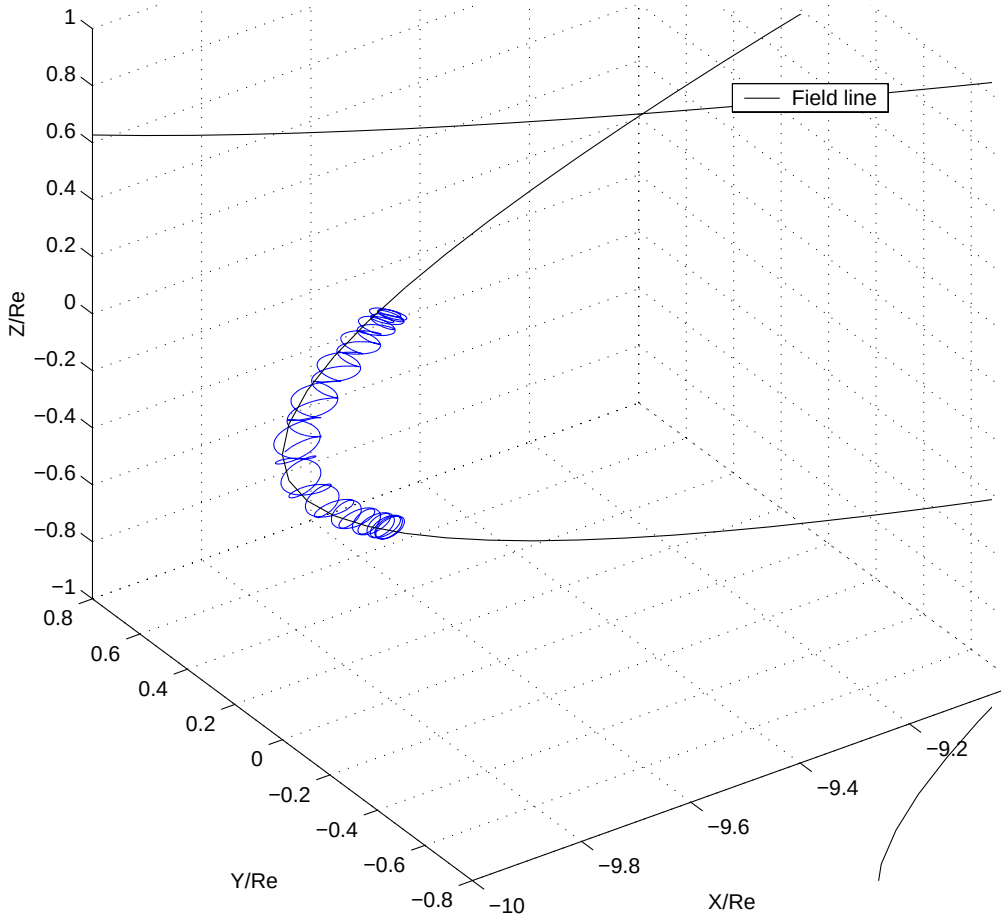

Figure 4.2: Parameters of Tsyganenko 96 model: P_{dyn}=3.0nPa, D_{st}=-50nT, B_y^{IMF}=0.0nT and B_z^{IMF}=10.0nT. The proton particle spirals along the magnetic field line for t=100s. The initial conditions are $\mathbf{X}$=(-10, 0, 0) R_E and $\mathbf{V}$=(438 km/s, $\psi = 60°$, $\theta = 60°$).

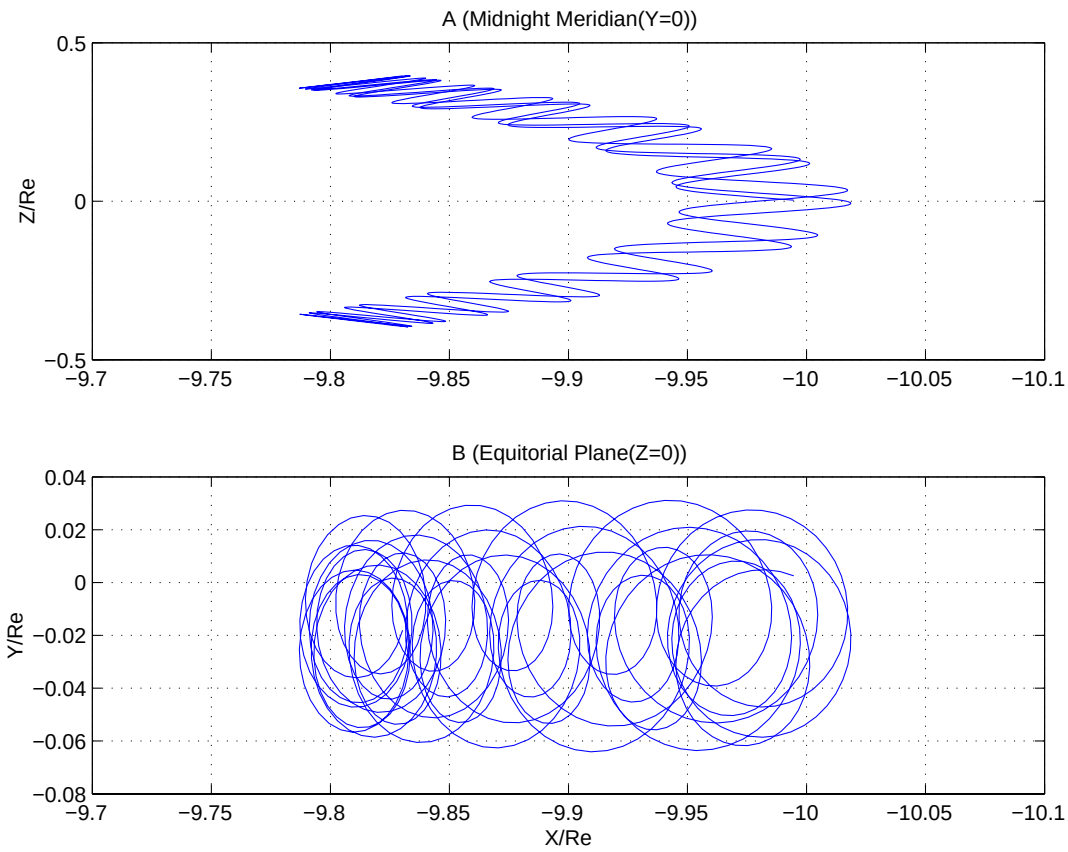

Figure 4.3: Parameters of Tsyganenko 96 model: P_{dyn}=3.0nPa, D_{st}=-50nT, B_y^{IMF}=0.0nT and B_z^{IMF}=10.0nT. The figure A is in midnight meridian; the figure B is in equatorial plane. The total orbit time shown is t=100 seconds and time-step of integrator δt=0.001 second. The orbit is the same proton orbit shown in figure 2. The Larmor radius r_L is around 0.03 R_E and $< \omega_c >$ is around 2.0 $1/s$. Thus there are approximately $< \omega_c >$t$/2\pi \approx 32$ cyclotron rotations.

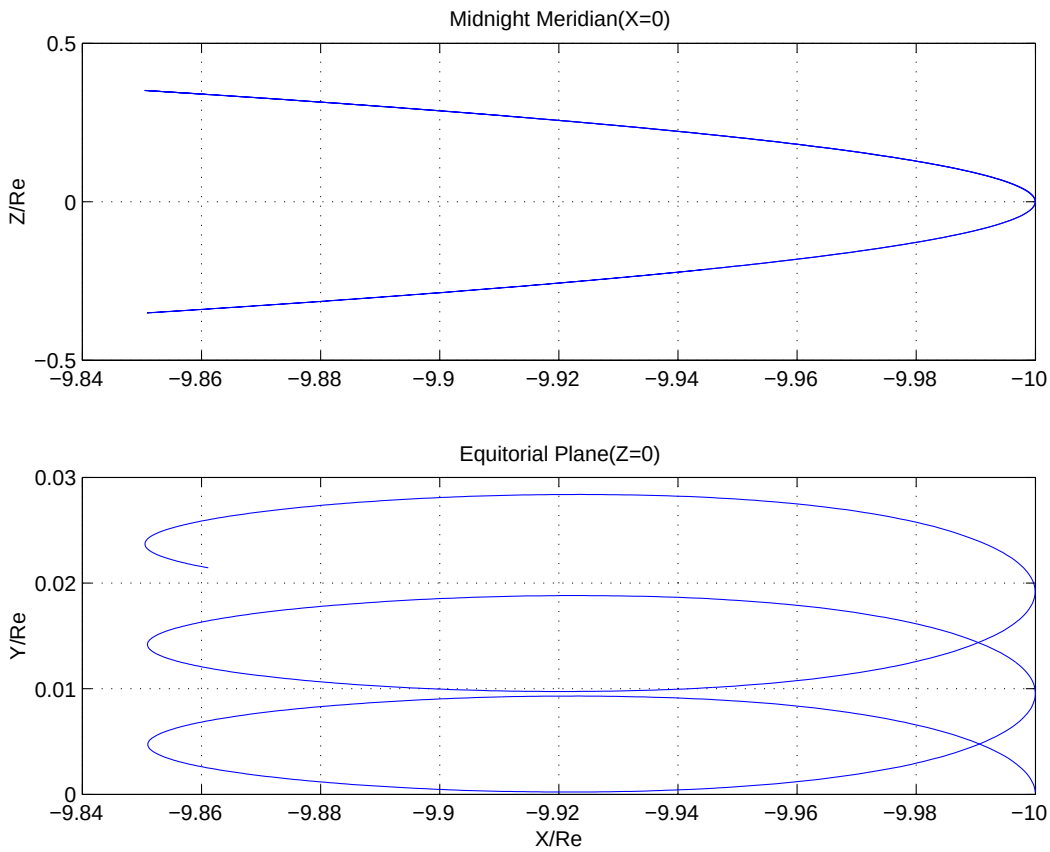

Figure 4.4: Parameters of Tsyganenko 96 model: P_{dyn}=3.0nPa, D_{st}=-50nT, B_y^{IMF}=0.0nT and B_z^{IMF}=10.0nT. This plot is the same initial conditions with figure 4.2 but using guiding center approximations. The upper plot is in midnight meridian; the bottom one is in equatorial plane. The initial values are $\mathbf{X} = (-10.0, 0, 0)\ R_E$ and $\mathbf{V} = (328.53, 189.68, 219.02)(km/s)$. The run time is 100 seconds and δt=0.1.

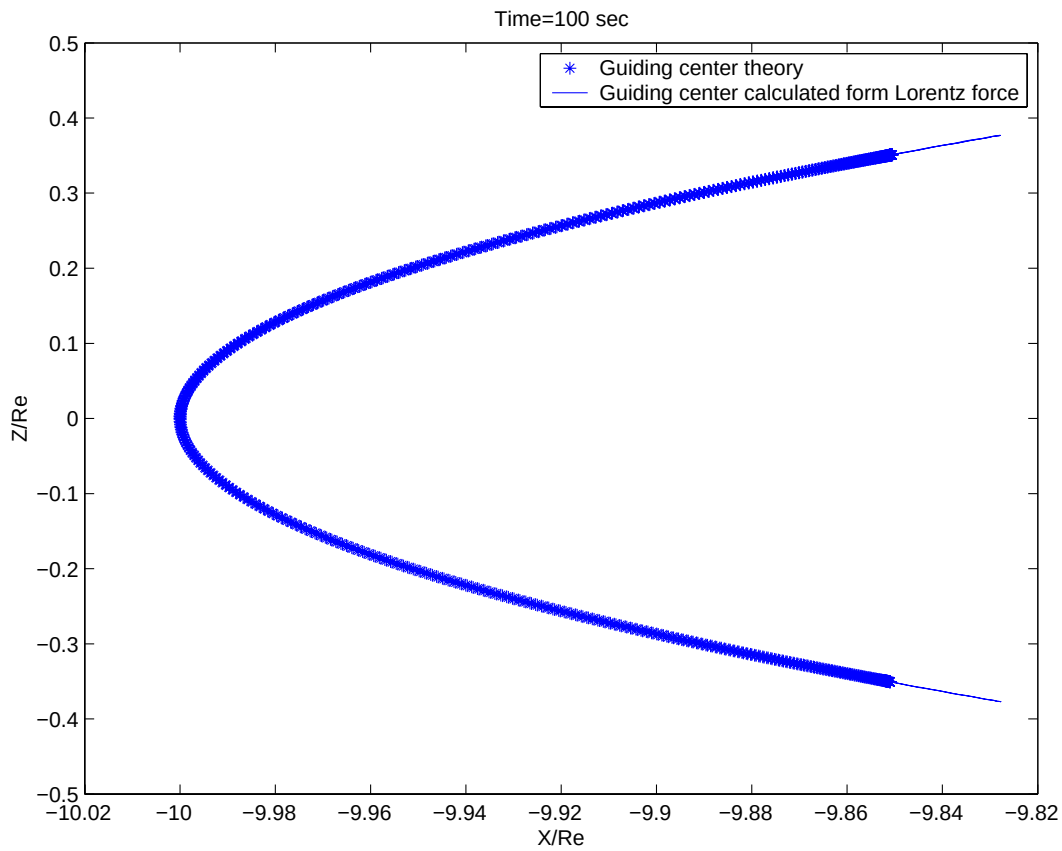

Figure 4.5: Direct comparison of the guiding center theory with the full Lorentz force. To do comparison we use equation (4.6) to compute $\mathbf{r_{gc}}(t)$ from $\mathbf{r}(t)$. Solid line means the calculation from Lorentz force equation. Dash line is estimated from guiding center theory directly. Direct compared of the guiding center orbit and guiding center calculated form Lorentz force orbits in equation (4.6) for a $1keV$ proton with $\mu = 0.044keV/\mathrm{nT}$. The mirror points a difference of $\triangle S/S = 0.02/9.84 = 2 \times 10^{-3}$.

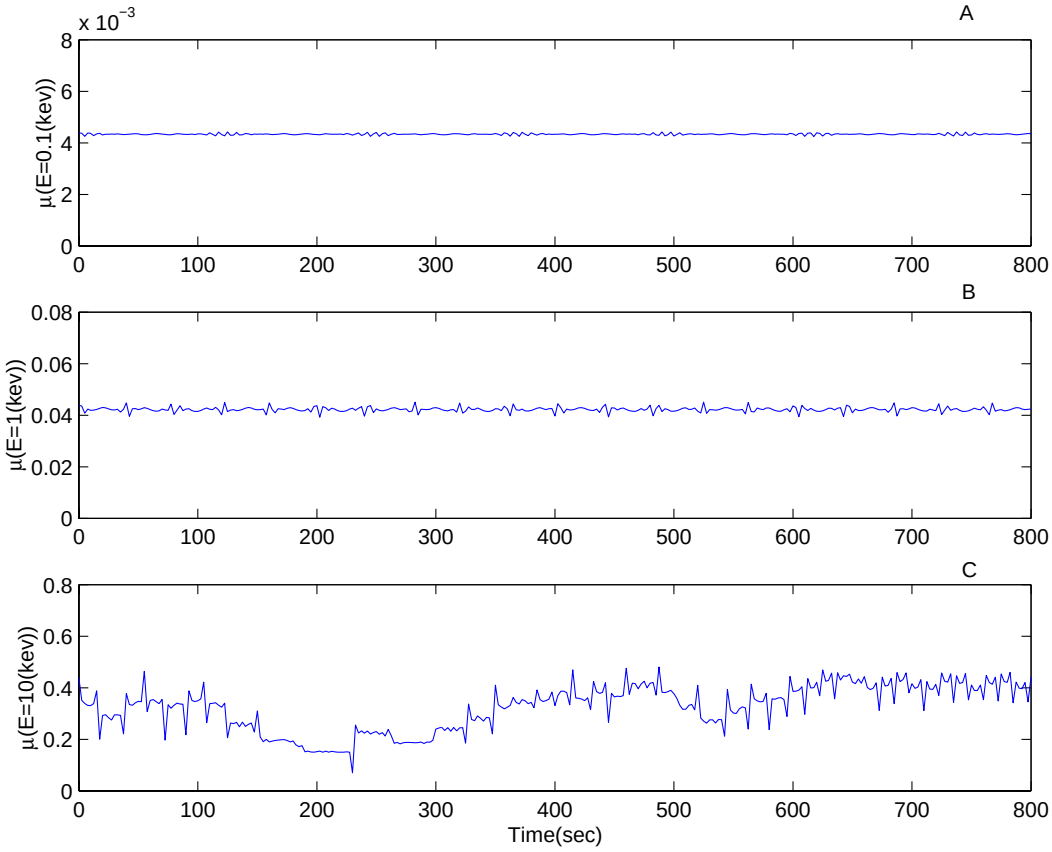

Figure 4.6: The initial pitch angle is 60° and gyrophase angle is 60°. The initial energies of figure 4.6A, 4.6B and 4.6C are $0.1keV$, $1keV$ and $10keV$ respectively. The unit of μ is keV/nT. The initial positions are all $\mathbf{X}$=(-10, 0, 0)R_E.

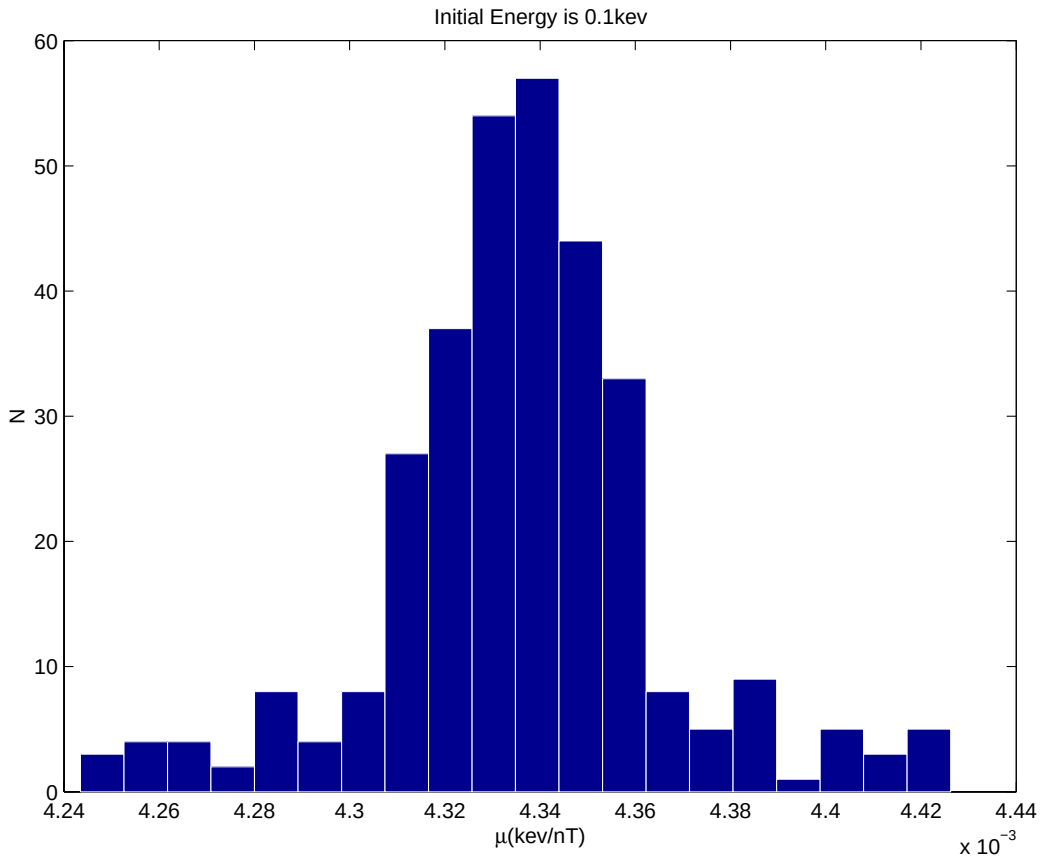

Figure 4.7: This figure shows the frequency of occurrence and their probability distribution $P(\mu)d\mu$ of value $mv_{\perp}^2/2B$ between the extreme $\mu_{\min}$ and μ_{max} with initial energy $0.1keV$. The distribution is approximately Gaussian with $<\mu>$=0.0043 and $\sigma_\mu = 2.95 \times 10^{-5}$ so that $\sigma_\mu/\mu = 6.8 \times 10^{-3}$.

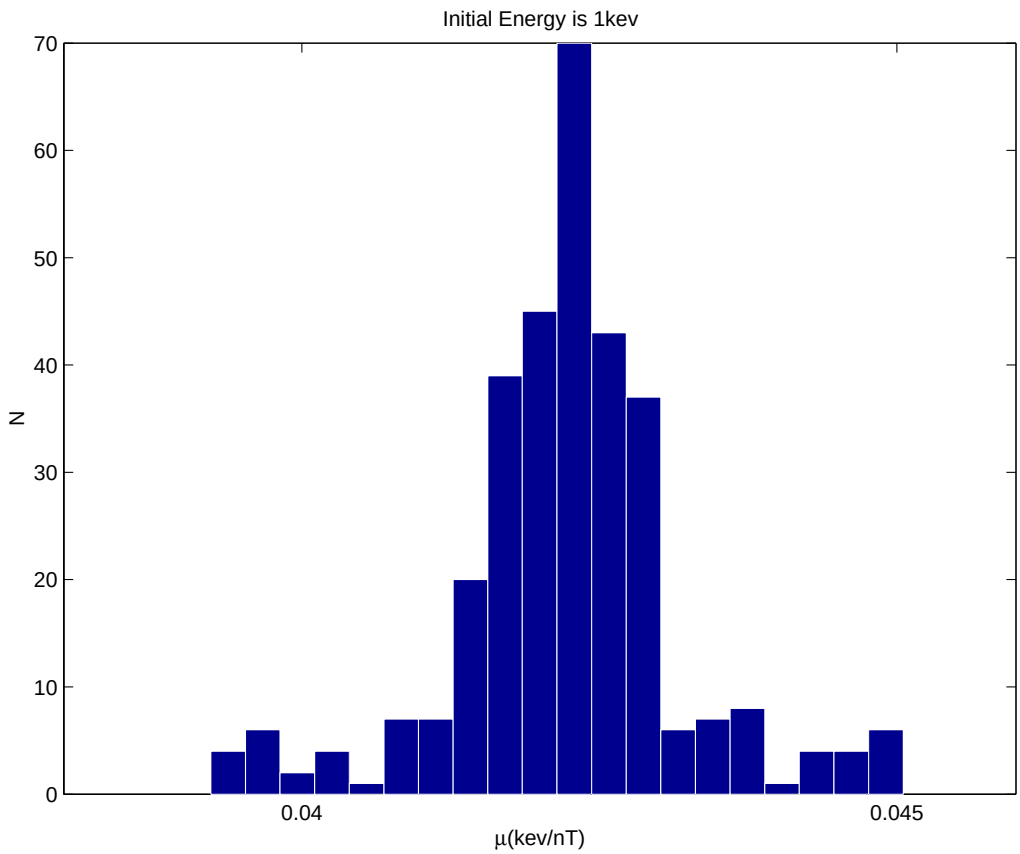

Figure 4.8: This figure shows the frequency of occurrence and their probability distribution $P(\mu)d\mu$ of value $mv_{\perp}^2/2B$ between the extreme $\mu_{\min}$ and μ_{max} with initial energy $1keV$. The distribution is approximately Gaussian with $<\mu>$=0.0422 and $\sigma_\mu = 9.5 \times 10^{-4}$ so that $\sigma_\mu/\mu = 0.0225$. The total number N of sampling points is 321 taken at every $\triangle t$=3.2s.

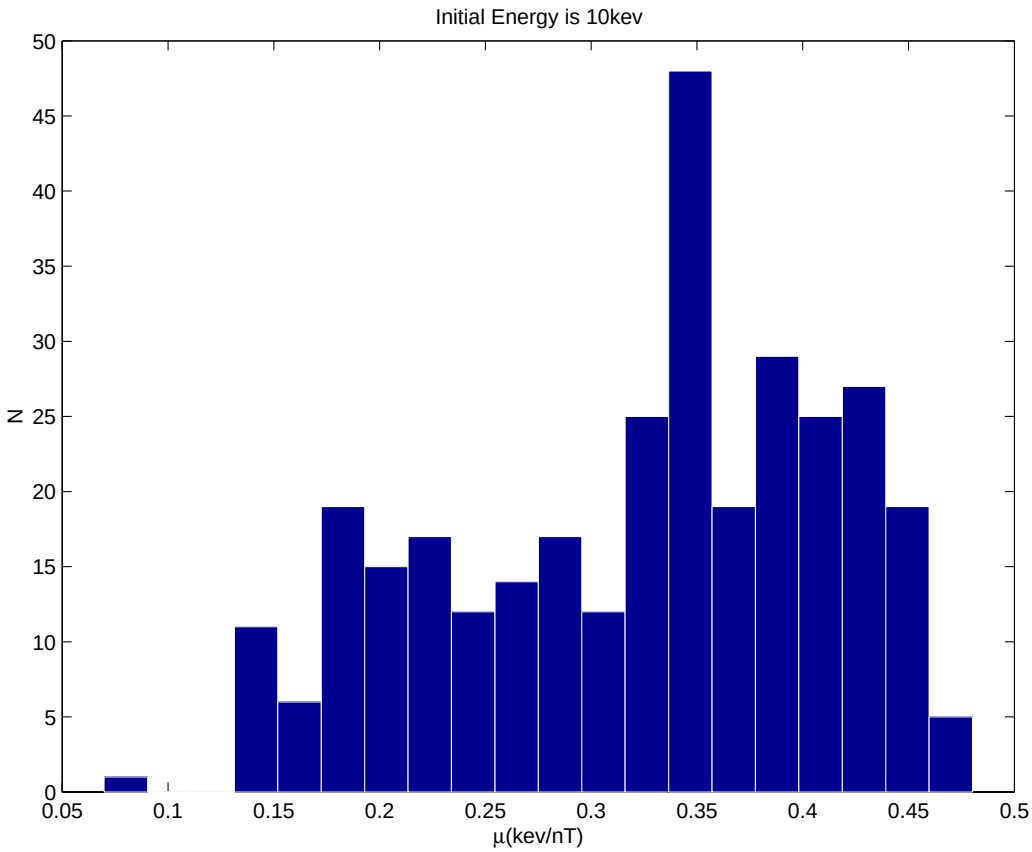

Figure 4.9: At $10keV$ the probability distribution $P(\mu)d\mu$ is now showing a non-Gaussian form with a wide box-like distribution. The distribution is approximately given with $<\mu>$=0.3236 and $\sigma_\mu = 0.0889$ so that $\sigma_\mu/\mu = 0.2746$. The kurtosis is small with $<\delta\mu^4>/<\delta\mu^2>^2 \approx 2.2$ and the skewness $s = <\delta\mu^3> / <\delta\mu^2>^{3/2} \approx -0.42$

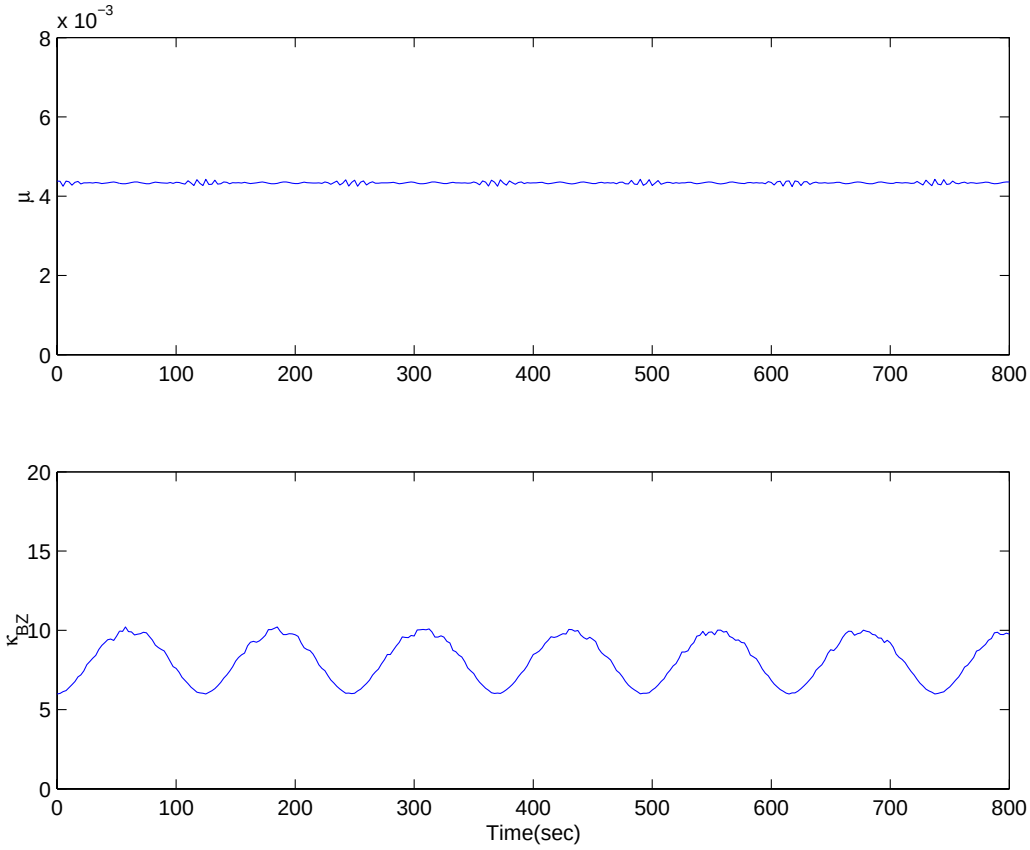

Figure 4.10: The top plot of the figure 10 is the magnetic moment μ versus time; the bottom one is the chaos parameter κ_{BZ} versus time. At $0.1keV$ the chaos parameter looks like a periodic function of time. The lower values of the chaos parameter show at the trough. The average magnetic moment $< \mu >$ is 0.0043 and σ_μ is 2.95×10^{-5}.

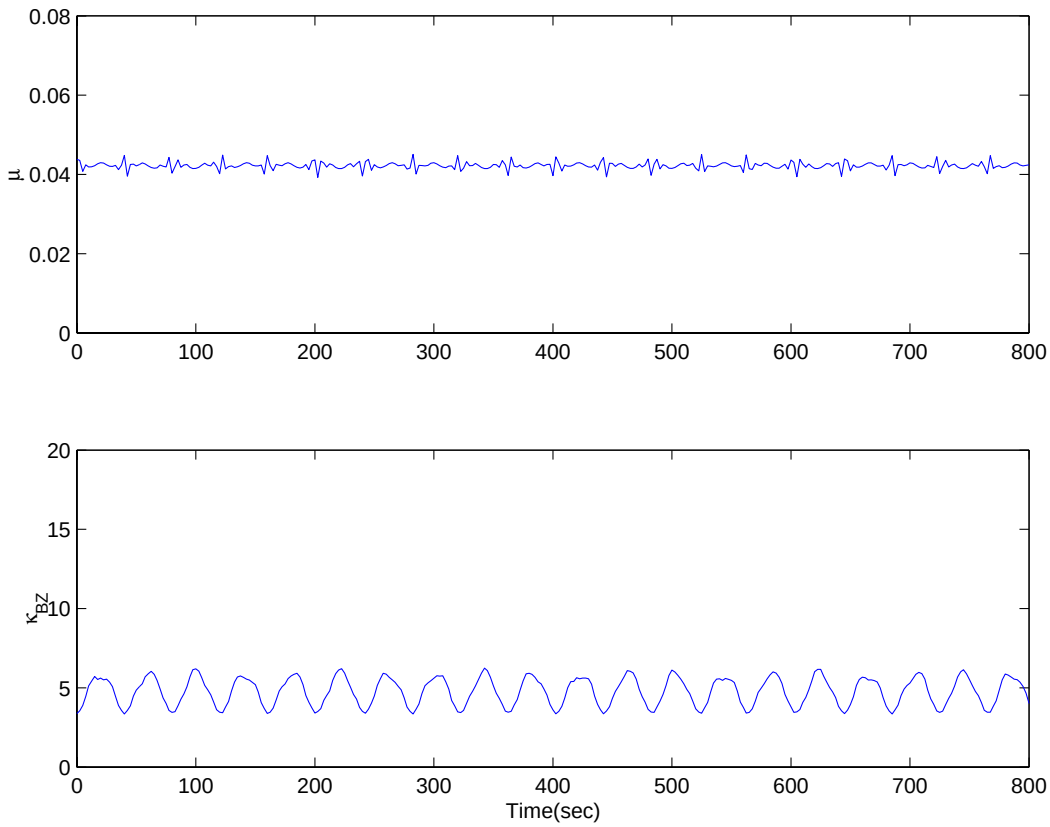

Figure 4.11: The top plot of the figure 10 is the magnetic moment μ versus time; the bottom one is the chaos parameter κ_{BZ} versus time. With increasing energy to 1 keV the magnetic moment μ responds more drastically than the previous one. But the small values still can be found at the trough. The chaos parameter κ_{BZ} versus time is similar to the periodic function. The average magnetic moment $< \mu >$ is 0.0422 and σ_μ is 9.5×10^{-4}.

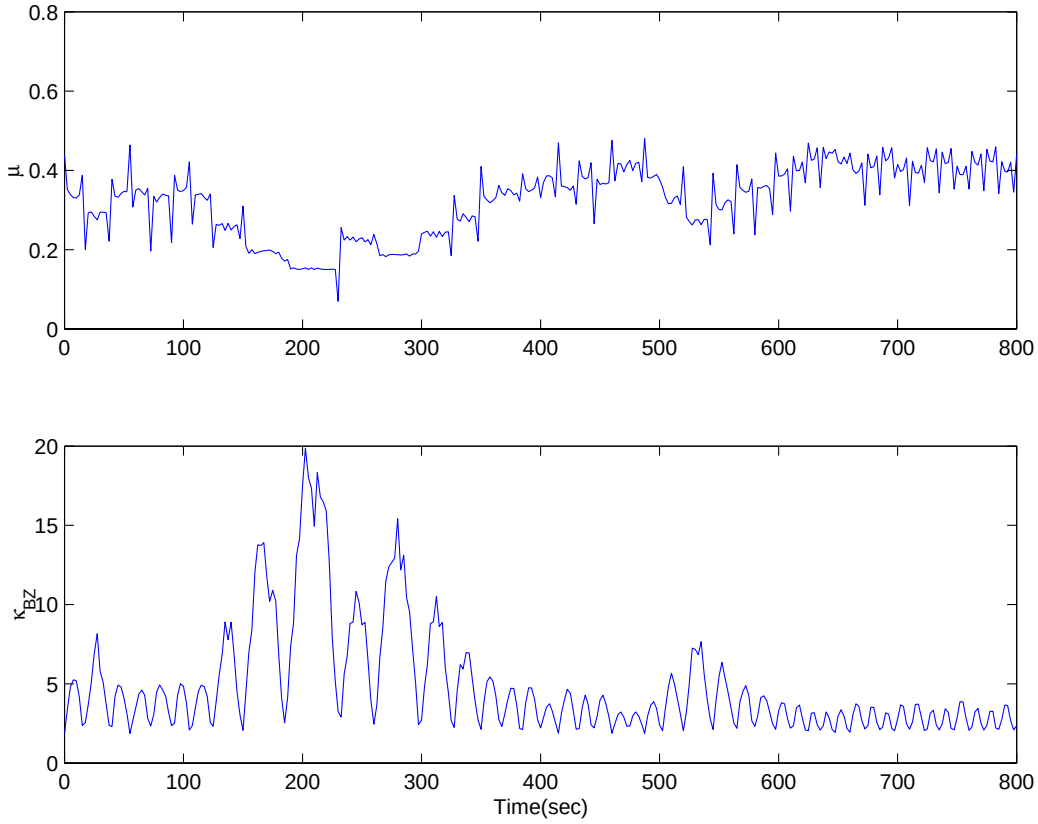

Figure 4.12: The top plot of the figure 10 is the magnetic moment μ versus time; the bottom one is the chaos parameter κ_{BZ} versus time. At $10keV$ with $<\mu>$=0.3236 and $\sigma_\mu = 0.0889$ the magnetic moment responds sharply when the particle crosses the neutral sheet. The chaos parameter versus time is non-periodic function of time. There are larger values of chaos parameter κ_{BZ} as smaller magnetic moment μ.

Chapter 5

Charged Particle Simulations

5.1 Energizing Mechanism

At section 4.5, the results we discussed are under no electric field $\mathbf{E} = 0$. The total energy is conserved in a magnetic field without electric field. However the magnetosphere contains substantial electric fields produced by the high velocity solar wind plasma blowing past the Earth's dipole magnetic field. The magnetospheric currents derived from Ampere's law applied to the measured magnetic fields in the lobe areas and their boundaries. The magnetotail of the earth contains a current sheet [21]. The magnetopause of the north and south lobes have currents I_N, I_S from the dusk to the dawn direction, where N and S stand for the north direction and the south direction respectively. The neutral sheet carries a dawn-to-dusk return current $I = I_N + I_S$, which is in the positive y direction under the GSE coordinates, that is in the dawn-to-dusk direction shown in figure 5.1. An electric field E_y exists in the same direction with the dawn-to-dusk current in y direction both at the magnetopause and in the central plasma sheet. The voltage drop across the geotail is $V(t) = E_y L_y$ and ranges from $40kV$ in quiet time to $800kV$ during substorms. We ask how much energy the particle can gain from the electric field E_y?

The dawn-to-dusk electric field is driven by the solar wind velocity v_x^{sw} and the IMF magnetic field $\mathbf{B}^{IMF}$. Derivation of the electric field is beyond the scope of this part of the work. The driven field is roughly $E_y \approx v_x^{sw} B_z^{IMF}$. For $v_x^{sw} = 400 km/s$ and $B_z^{IMF} = 10$nT this gives $E_y = 4mV/m$.

Particles acquire energy during the times they are in the quasi-neutral sheet.[15]. After equation (4.1) times $\mathbf{v}$ we derive:

$$\frac{d}{dt}(\frac{1}{2}mv^2) = q\mathbf{v} \cdot \mathbf{E}. \tag{5.1}$$

This formula is the same as equation (4.5) at chapter 4.2. The equation can be also rewritten as

$$\triangle W = \triangle(\frac{1}{2}mv^2) = q\mathbf{v}\triangle t \cdot \mathbf{E} = q\triangle \mathbf{x} \cdot \mathbf{E} \tag{5.2}$$

for the increase of energy $\triangle W$ in a time interval $\triangle t$ restricted only by the requirement that $\mathbf{E}$ is constant over that time interval. This formula states that the particle obtains the energy as long as the particle has a displacement parallel to the direction of electric field. The particles are accelerated by the dawn-dusk electrical field $E_y(t)$ and spouted out from the quasi-neutral layer at which dawn-dusk electric field $E_y(t)$ occurs [12]. Therefore the particles gain energy proportional to the displacement $\triangle \mathbf{x}$ in the y direction, contributed by $\triangle y$. Since the orbits are complicated it usually requires numerical solutions to determine the $\triangle y$ displacement.

The geo-magnetic field models we work within this section are the function of positions, but not a function of time. According to Faraday's law, which is

$$\nabla \times \mathbf{E} = -\frac{\partial \mathbf{B}}{\partial t}, \tag{5.3}$$

$\partial \mathbf{B}/\partial t$ is zero because magnetic field is not the function of time. Consequently $\nabla \times E = 0$ implies the electric field does not vary with space. Thus the electric field we discuss is a function of time, $E_y(t)$ alone. Another interesting class of fields that are complex function of space and time is developed by *Shin Lin Li* and *Baker et al.*

In the next section we want to discuss two classes of the electric fields: the constant electric field and the electric field as a function of time. The electric fields are assumed to be independent on space, that is uniform throughout the geotail region. The magnetic field model we apply is the Tsyganenko 96 model.

5.2 Energization from Constant Solar Wind

Particles experience a force due to electric field and drift toward the earth by Lorentz force equation. The transverse action $S_\perp$, which is perpendicular to the direction of particle motion,

$$S_\perp = \oint p_\perp \cdot dq_\perp \tag{5.4}$$

taken over a period of the transverse oscillation is an adiabatic invariant as the particles drift into regions of a changing transverse field gradient ($q_\perp$ and $p_\perp$ are the position and momentum vectors).[22] From the invariant of $S_\perp$, particles moving in a field with increasing transverse field gradient gain transverse oscillation energy at the expense of the kinetic energy in the field line ($\hat{b}$) direction.

As an example we take both the pitch angle and the gyrophase angle are 60°. The magnetospheric parameters of Tsyganenko 96 model are $P_{dyn} = 3.0$nT, $Dst = -50$nT, $B_y^{IMF} = 0.0$nT and $B_z^{IMF} = 10.0$nT. We take the reference value of the electric field as $E_y = 1mV/m$ through out the magnetosphere (magnetotail).

5.2.1 E_y is constant

Under the constant electric field $E_y = 1mV/m$ the particle gains energy and drifts toward the earth while doing gyro-motion along the magnetic configurations.Table 5.1 shows the initial condition of these simulations. Figure 5.2 and figure 5.3 show the particle drifts starting from the current sheet, the north lobe and the south lobe in the meridian plane and equatorial plane respectively within a hour (3600 seconds). The particle starts to drift with different initial energies at three different positions (-25, 0, 0), (-25, 0, 3) and (-25, 0, -3). The higher the energy of the protons, the higher initial velocity and particle drifts. The pitch angle is 60° and gyrophase angle is 90° in all

Initial Position(x, y, z)	(-25, 0, $\pm$3) (-25, 0, 0) R_E
Pitch Angle ψ	60°
Gyrophase Angle θ	90°
Initial Energy	$0.1keV$, $1keV$ and $10keV$
Electric Field	$1mV/m$

Table 5.1: The initial conditions of the particle in 5.2.1

events. The charged particle still drifts toward the earth and bounces back and forth wherever it starts in the meridian plane. The mirror points are closer and closer to the earth. With increasing initial energy the particle can float for a longer distance. With larger initial energy the particle tends to drift around the earth as it gets close to the earth. When the particle drifts to about $2R_E$ gravity is around 4×10^{-27}N and does not influence the particle. The Lorentz force is about $10^{-18} \sim 10^{-20}$N larger than gravity. The $10keV$ ions reach around X=-$2R_E$ and then drift to the evening sector. This takes about 30 minutes when particles drift to evening sector from x=-$25R_E$.

Figure 5.4 shows that the change W versus time. At lower energy, the particle drifting from the north and the south lobe do not acquire much energy because ions do not have distant displacement in the y direction, corresponded with subplots in figure 5.3. The protons acquire about $50keV$ wherever they start to drift with the initial energy of the particle $10keV$. But the the energy drops as particles pass by the Earth. Thus particles have larger energies when drifting close to earth. These energies are released into the ring current area. We can obtain similar results either from calculating equation (5.2) or from

$W = 0.5mv_{\parallel}^2 + 0.5mv_{\perp}^2$ with initial energy $10keV$, as shown in figure 5.5.

The velocity of initial energy $0.1keV$, $1keV$ and $10keV$ are around $139km/s$, $438km/s$ and $1385km/s$ respectively. The initial energy determines the original drift velocity of the particle. Thus the ions obtain more energy if the particle possesses more initial energy. With the higher initial energy the magnetic moment μ changes strongly, which is shown in figure 5.6. The magnetic moment μ varies when the particle intersects the neutral sheet. Figure 5.7 shows the probability distribution of the magnetic moment μ. When the initial energy is small, the probability distribution is similar to Gussian distribution. However, the particle starting to drift from the South lobe has the smaller magnetic moment μ. Thus the figure, which the particle starts to drift from the South lobe with initial energy $0.1keV$, is similar to Possion distribution. With the higher initial energy the probability distribution looks like non-Gaussian distribution. The magnetic moment μ is close to a constant around $0.1keV$/nT when drifting close to the earth because the strength of the magnetic field around the earth is much larger.

With the same initial energy $1keV$ particles possess different orbits under different gyrophase angle θ, as indicated in figure 5.8 and figure 5.9. In the equatorial plane the line connected angle 180° and 360° separates the plane into two parts, dayside area and nightside area. The gyrophase angle 60° and 120° are in the dayside region; 240° and 300° are in the nightside region.

Initial Position(x, y, z)	(-25, 0, ± 3) (-25, 0, 0) R_E
Pitch Angle ψ	60°
Gyrophase Angle θ	90°
Initial Energy	$10keV$
Electric Field	1 (mV/m) $t \leq 30mins$
	-1(mV/m) $t > 30mins$

Table 5.2: The initial conditions of the particle in 5.2.2

Figure 5.10 shows the total energies acquired from equation (5.2) versus time. Particles drifting from the nightside area obtain more energy. And particles possess higher magnetic moment μ drifting from the nightside region, indicated in figure 5.11. Thus particles are easy to escape with increasing initial energy if particles start to drift in the nightside.

5.2.2 E_y is constant but changes direction after some time

With the higher initial energy particles drift closer to the Earth. Particles drifting close to the Earth spend around 30 minutes. What happens to particles if the electric field changes strongly to the opposite direction from the original electric field? We suppose that the electric field is $1mV/m$ and changes to -$1mV/m$ after 30 minutes. The detail initial conditions are in table 5.2.

Figure 5.12 are the plots of the particles' orbits shown in the two-dimensions, equatorial plane and meridian plane. Particles arrive to the

dusk area in the equatorial plane around 30 minutes. The ions obtain energies around $50keV$. Particles seem to drift backward when the electric field changes. From the second column of the figure 5.13 the magnetic moment μ is stable. The chaos parameter κ_{BZ} does not change sharply after 30 minutes. Particles seem to be trapped in the dusk area in the equatorial plane. Particles gaining the energy are independent on the position where the particles start to drift. More energy releases into the ring current than the energy under the constant electric field. The energies of particles drop around $10keV$. Thus particles relieve more energy when the electric field changes to the opposite direction.

5.3 Energization from Variable Solar Wind

According to Ampere's law the displacement current is quite small compared with the induction current in the geotail region. Voltage drop across the magnetic tail is around $800kV$ within the substorms. During the substorms the electric filed ($E_y = V/L_y$) is about $6.25mV/m$ with the width of the magnetosphere $L_y = 20R_E$. When ions drift close to $1.5 \sim 5R_E$, the displacement current is around $10^{-18} \sim 10^{-20}(A/m^2)$ much smaller than conduction current $10^{-9}(A/m^2)$. Thus the influence of displacement current on the magnetic field does not need to be considered.

With the solar wind passing by the electric field changes with time

Initial Position(x, y, z)	(-25, 0, 0) R_E
Pitch Angle ψ	60°
Gyrophase Angle θ	90°
Initial Energy	$10keV$

Table 5.3: The initial conditions of the particle of section 5.3

increasing. I simulate the particle motion by using the electric field similar to the Gaussian distribution as

$$E_y = \frac{\alpha}{\sqrt{2\pi}} exp[-\frac{(t - t_{\mathrm{E_{max}}})^2}{2\sigma}], \tag{5.5}$$

where t means the time in second, $\sigma = 10^6 s^2$ and $t_{\mathrm{E_{max}}} = 2000s$ stands for the electric field has the maximum value as $t = 2000s$. After 2000 seconds the electric field gradually drops close to 0. The maximum electric field is close to $1mV/m$ when $\alpha = 2.4$. The detail initial conditions are shown in table 5.3.

In figure 5.14 and figure 5.15 the particle drifts for 2.5 hours with the electric field from equation (5.5). The particle arrives close to the earth around 1.1 hours ($4000s$). Figure 5.14 plots shows orbit positions and time. The figure 5.15C indicates that energy drops around 5$\sim$10keV as time= $4000s$. The magnetic moment μ also falls because the energy drops. Within 4000 to 6000 seconds the particle drifts in the dayside and turns around the Earth. Ions cost around 2000 seconds drifting the dayside area. The chaos parameter κ_{BZ} perturbed sharply when the particle drifts in the dayside area, which is indicated in figure 5.15D. After 6000 seconds the particle drifts back to the

nightside region. But the electric field is very small. The particle drifts back to the geotail and does the gyromotion toward to the Earth again.

5.4 Comparisions with Solar Flare Energization

The corona is the outermost atmosphere of the sun. The corona is located above Chromosphere with a density of $10^{15}m^{-3}$ near the sun. The temperature increases abruptly to 2×10^6K in the corona from the 6000K Photosphere through the transition region. The corona is an active region and its magnetic field is the strongest on the sun. Sometimes a solar flare is rapidly generated in the corona. Solar flares are easily observed during the solar eclipse. Coronal mass ejections may happen along with an associated flare or eruptive prominence. Neither solar flares nor prominence eruptions are the reason to cause coronal mass ejections [16]. A solar flare is associated with the coronal loops, which is a closed magnetic field line connected to magnetic regions on the solar surface. Coronal loops are found around the sunspots in active regions. Charged coronal gas is trapped from relatively dense region by closed magnetic field lines. Many coronal loops can last for days or weeks but change quickly. The density of the coronal loops is higher than in other regions. The observed properties of the solar wind near the earth (1AU) are in table 5.4. More detail on the solar wind parameters are given by *Hundhausen*, in p.93 in the *Rusell* and *Kivelson* book.

Soft x-ray pictures clearly show the coronal loops and bright points,

Proton density	$6.6\ cm^{-3}$
Electron density	$7.1\ cm^{-3}$
Flow speed	$0.25\ km \cdot s^{-1}$
Proton Temperature	1.2×10^5K
Electron Temperature	1.4×10^5K
Magnetic field	7×10^{-9}T

Table 5.4: Properties of the solar wind observed near the earth (1 AU) [21]

where magnetic fields interact. New higher resolution images of coronal loops and solar flares are found at http://vestige.lmsal.com/TRACE/Public/Images/ taken by soft x-ray cameras on the *Transition Region and Coronal Explorer* (TRACE) satellite launched by the Naval Research Laboratory in April, 1998. TRACE includes 1024×1024 CCD detector and gathers over 8.5×8.5 arc minute images. After the Solar Maximum Mission, TRACE is the first satellite related with solar research in the United States. Solar physicists can learn the connections between solar magnetic field and related plasma properties to the sun by observing the photosphere, the transition region, and the corona. Many space problems, such as reconnection, plasma heating and wave propagation, happen in the atmosphere of the sun. We can learn the details of research about energy mechanism in stellar studies.

Chen and Shibata [3] proposed the solar flare magnetic flux ψ can be decomposed into a background field ψ_b flux, magnetic field caused by image current ψ_i flux, and magnetic field from a line current ψ_l flux. In local x, y coordinates with x measured horizontally at the surface of the photosphere and

y vertically upward, the three components are given in units $x \to xL_\circ, y \to yL_\circ$ with $L_\circ = 10^5$ km and $\psi \to B_\circ L_\circ$ by $B_\circ = 100G = 10^{-2}T$. The plasma β is chosen to be 0.01 corresponding to Alfvén wave speed v_A 1818 kms^{-1}. The time scale is $L_\circ/v_A$ around 55s. The components can be described as:

$$\psi_b = I(t) ln \frac{[(x+0.3)^2 + (y+0.3)^2][(x-0.3)^2 + (y+0.3)^2]}{[(x+1.5)^2 + (y+0.3)^2][(x-1.5)^2 + (y+0.3)^2]} \tag{5.6}$$

$$\psi_i = -\frac{B_i r_o}{2} ln[x^2 + (y+h)^2] \tag{5.7}$$

$$\psi_l = \begin{cases} B_l r^2/2r_o, & r \leq r_o; \\ B_l r_o/2 - r_o ln(r_o) + r_o ln(r), & r > r_o. \end{cases} \tag{5.8}$$

where I(t) is the current model of the solar background emerging flux from two line dipole at positions. The positions (±1.5, -0.3) and (±0.3, -0.3) are the solar dipole under the photosphere. h, depth of the image current, is equal to 2 and with $r = [x^2 + (y-h)^2]^{1/2}$. The radius of the line current is $r_o = 0.5$. The magnetic field is found by relation with flux ψ by

$$\mathbf{B} = \nabla\psi \times \hat{\mathbf{z}}. \tag{5.9}$$

A simple picture of the mass ejection is produced by assuming the current model $I(t)$ is the hyperbolic function of time $I(t) = sech(2\pi t/100)$ where t is time because the current decreases with time when mass ejects. In the simulation shown in figure 5.16, we keep the line current $B_l r_\circ$ and image current $B_i r_\circ$ constant. According to Ampere's law,

$$\oint B \cdot dl = \mu_\circ I. \tag{5.10}$$

Thus current I=1 means $2\pi B_\circ L_\circ/\mu_\circ = 5 \times 10^{12}$A. The emerging flux from the two line dipole currents is smaller and smaller as time increases. Emerging flux triggers coronal mass ejections. The flux is under a balance between magnetic buoyancy and magnetic tension. Energy can be stored in the top of the inner configuration bubble at the initial time (time is 0 second), indicated in figure 5.16A. In figure 5.16B at t=8 the field lines start to break and reconnect. Coronal mass ejections release mass and energy in a very short time scale. The mass from coronal ejections can increase the strength of the magnetic field. Reconnection point is increasing and causes the location of field loops to rise [21]. The configuration loops of chromosphere move apart. Thus, field lines grow with mass ejections coming and passes energy into the instellar medium. The sequential plot of figure 5.16 shows the growing condition of the field line with time increasing. The simple reconnection process is shown in figure 5.17.

We simulate the particle motion in coronal mass ejections by using the Lorentz force under the magnetic field of the corona. The particle drifts and mirrors back along the coronal magnetic configuration, as indicated in figure 5.18. From the bottom plot of figure 5.18 the particle drifts lower and lower from the equatorial plane. The particles do the gyromotion along the field line of the corona. The background current is the function of time as shown in figure 5.15. The particles in the corona are released into the space doing the gyromotion with eruptive prominence as time increasing.

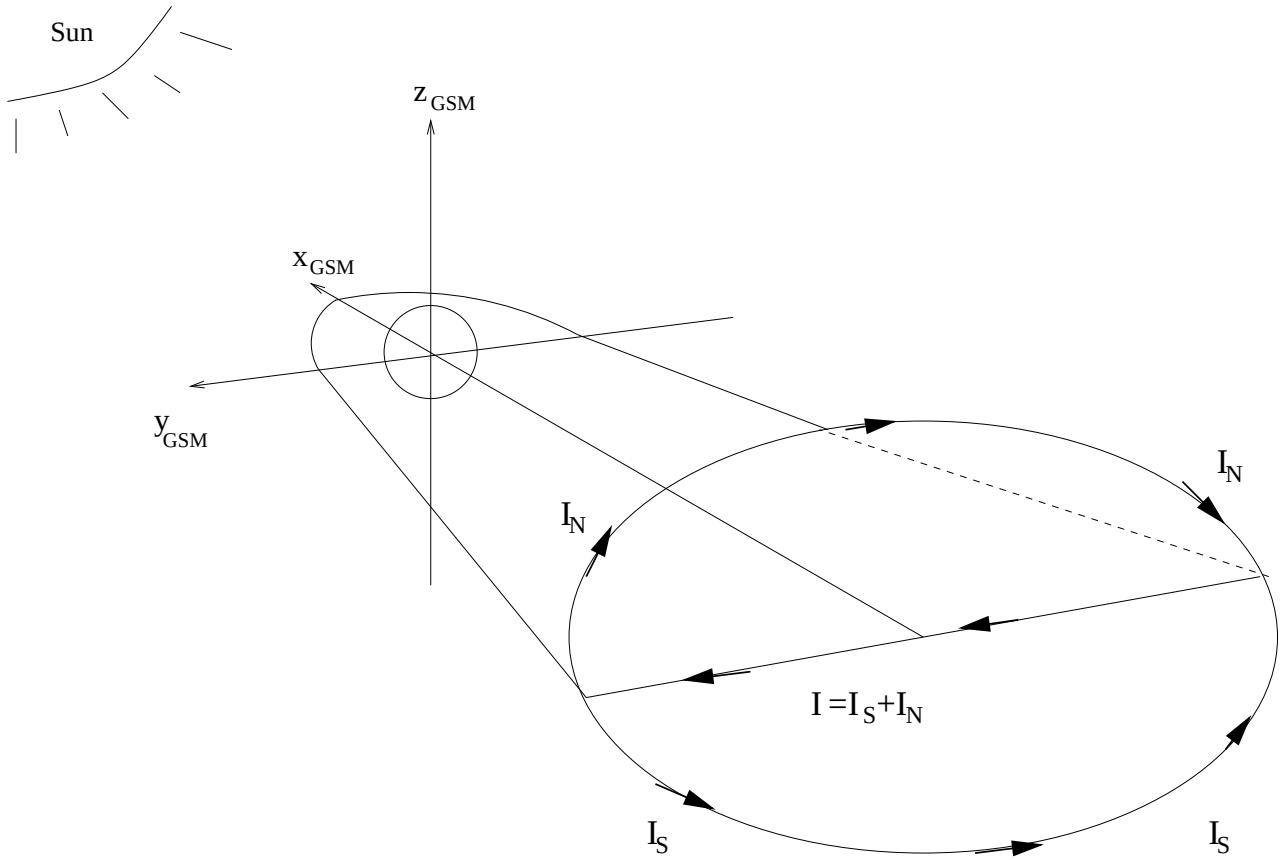

Figure 5.1: When the particle enters the magnetopause through reconnection, it can generate a dawn-to-dusk current in the geotail. This figure displays the configuration of the current.

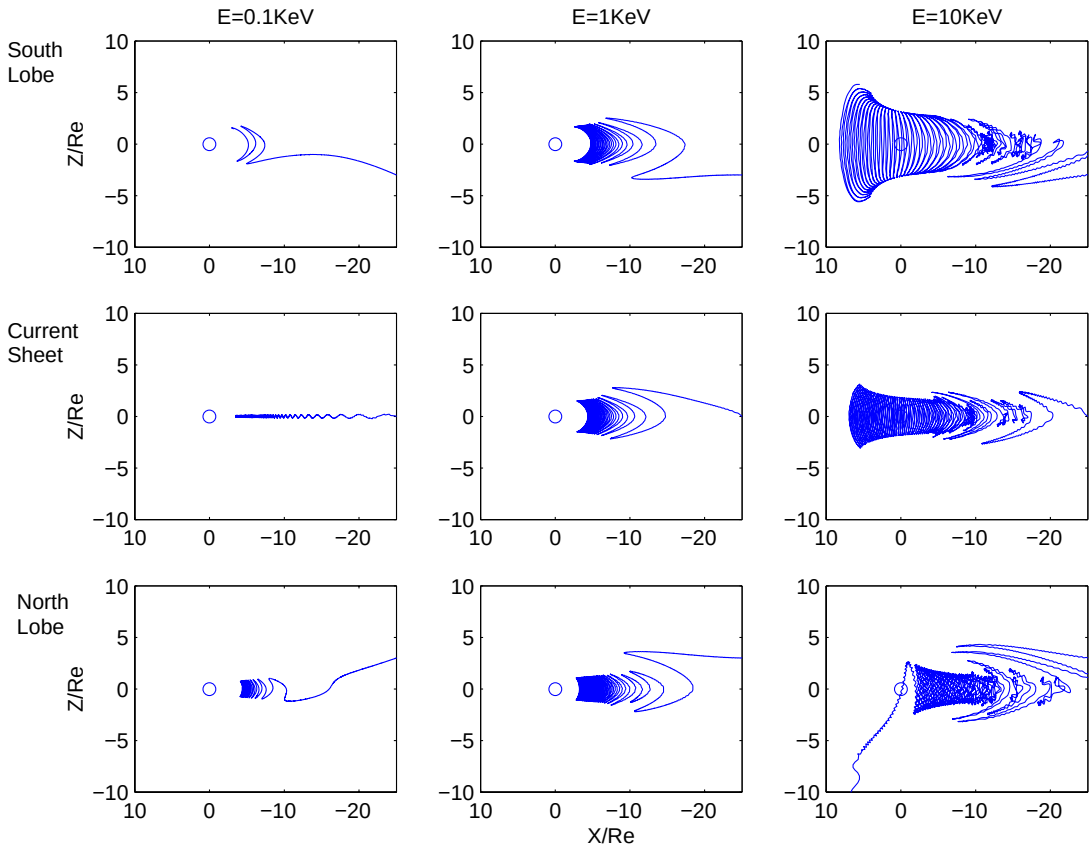

Figure 5.2: Parameters of Tsyganenko 96 model: P_{dyn}=3.0nPa, D_{st}=-50nT, B_y^{IMF}=0.0nT and B_z^{IMF}=10.0nT. With initial pitch angle $\theta = 60°$ and gyrophase angle $\psi = 90°$ the particle starts to drift from the north lobe, the current sheet and the south lobe with constant electric field in y direction ($E_y = 1mV/m$) individually. The first row show protons that drift from the south lobe with different initial energies. The second row particle shows protons that drift from the current sheet. The third row shows protons that drift from the north lobe. Starting points **X** from the north lobe, the south lobe and current are (-25, 0, -3), (-25, 0, 0) and(-25, 0, 3) respectively. These figures are shown in meridian plane.

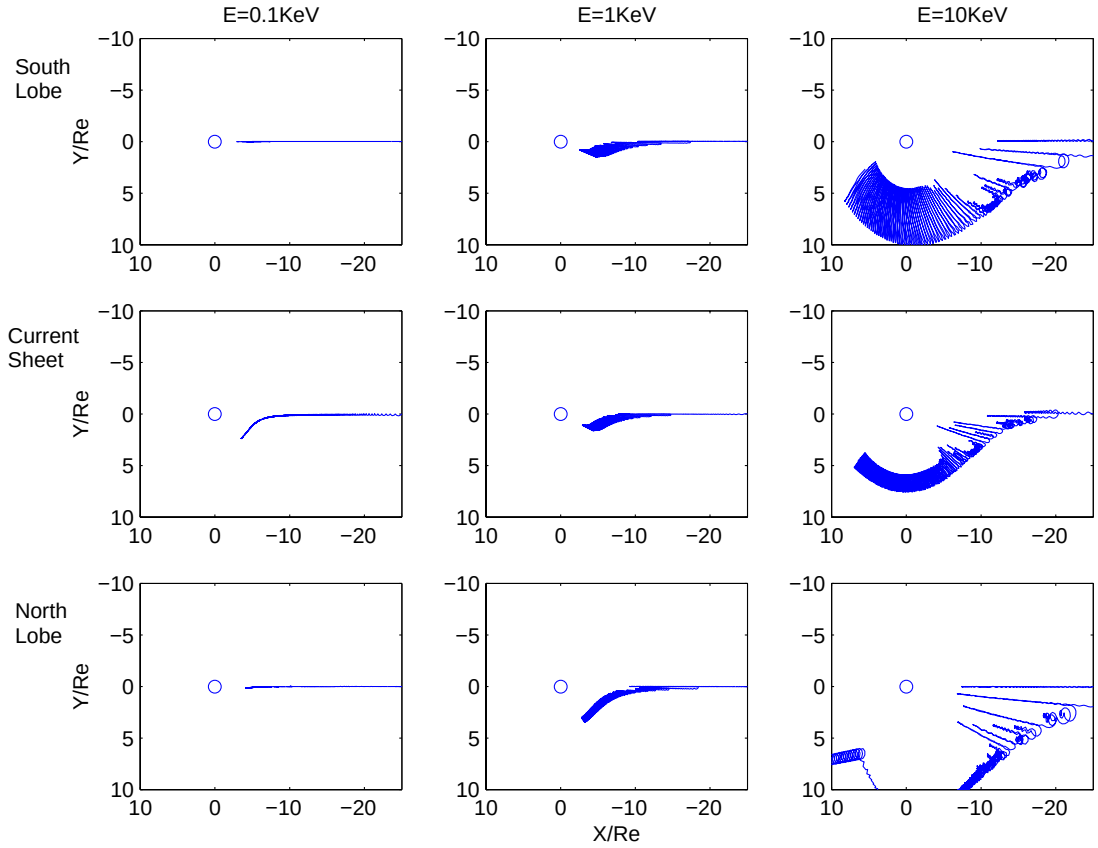

Figure 5.3: Parameters of Tsyganenko 96 model: P_{dyn}=3.0nPa, D_{st}=-50nT, B_y^{IMF}=0.0nT and B_z^{IMF}=10.0nT. With initial pitch angle $\theta = 60°$ and gyrophase angle $\psi = 90°$ these plots are displayed in equatorial plane under the same parameters with figure 5.2. These plots look down from the north pole.

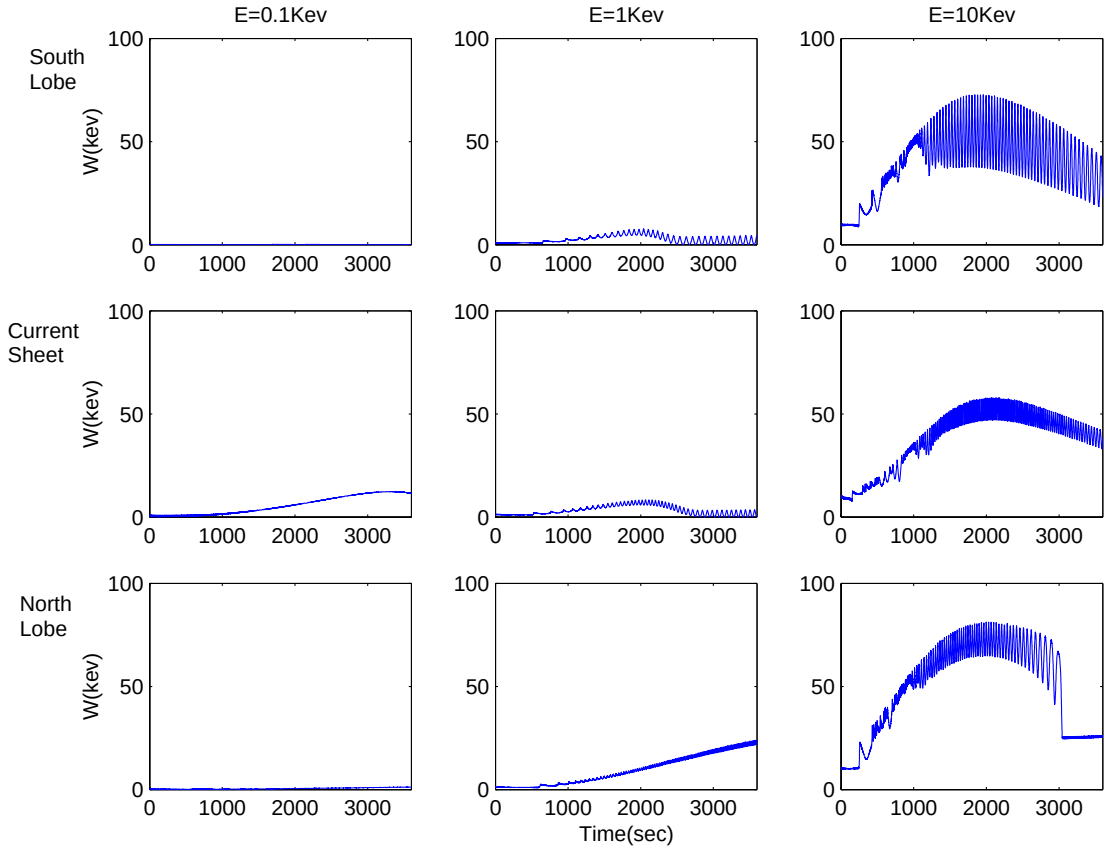

Figure 5.4: Parameters of Tsyganenko 96 model: P_{dyn}=3.0nPa, D_{st}=-50nT, B_y^{IMF}=0.0nT and B_z^{IMF}=10.0nT. With initial pitch angle $\theta = 60°$ and gyrophase angle $\psi = 90°$ these plots display the total energy W versus time in second. The unit of energy is in keV.

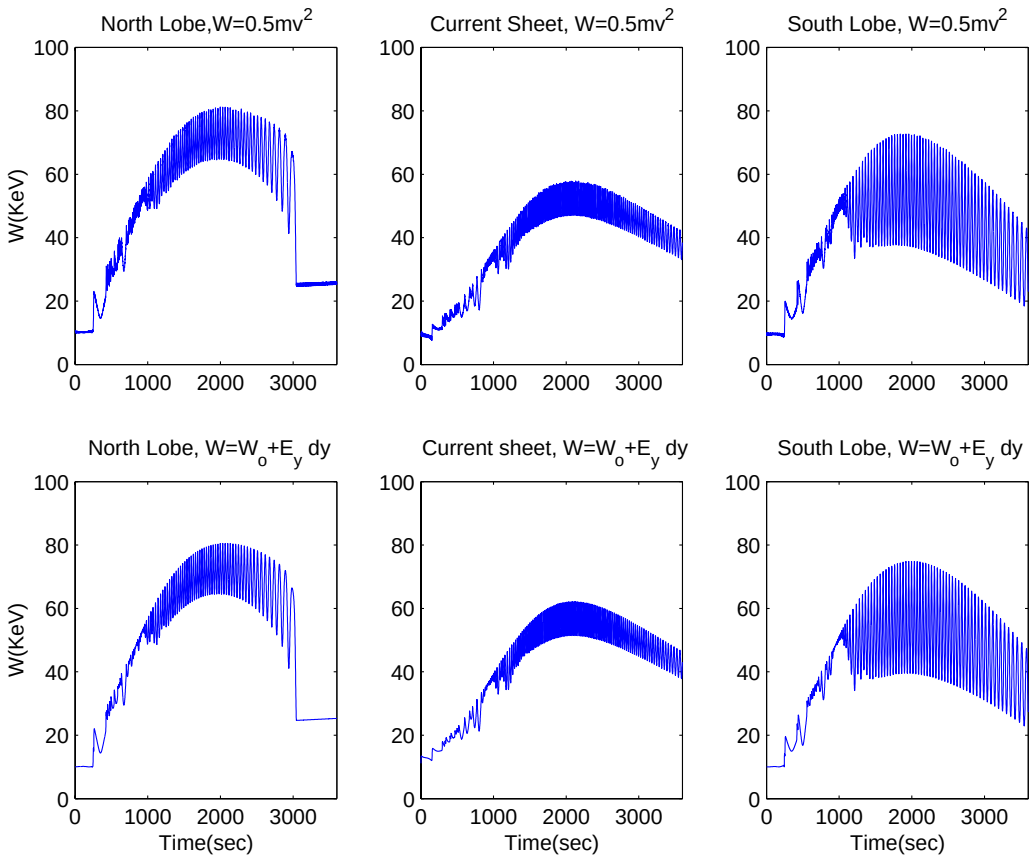

Figure 5.5: The values of these plots are energy versus time calculated from two methods. Plots in the first row are calculated from $W = mv^2/2 = mv_{\|}^2/2 + mv_{\perp}^2/2$. The second row comes from the integrating equation (1) to get equation (2) with $E_y = 1mV/m$=constant. The unit of energy is keV.

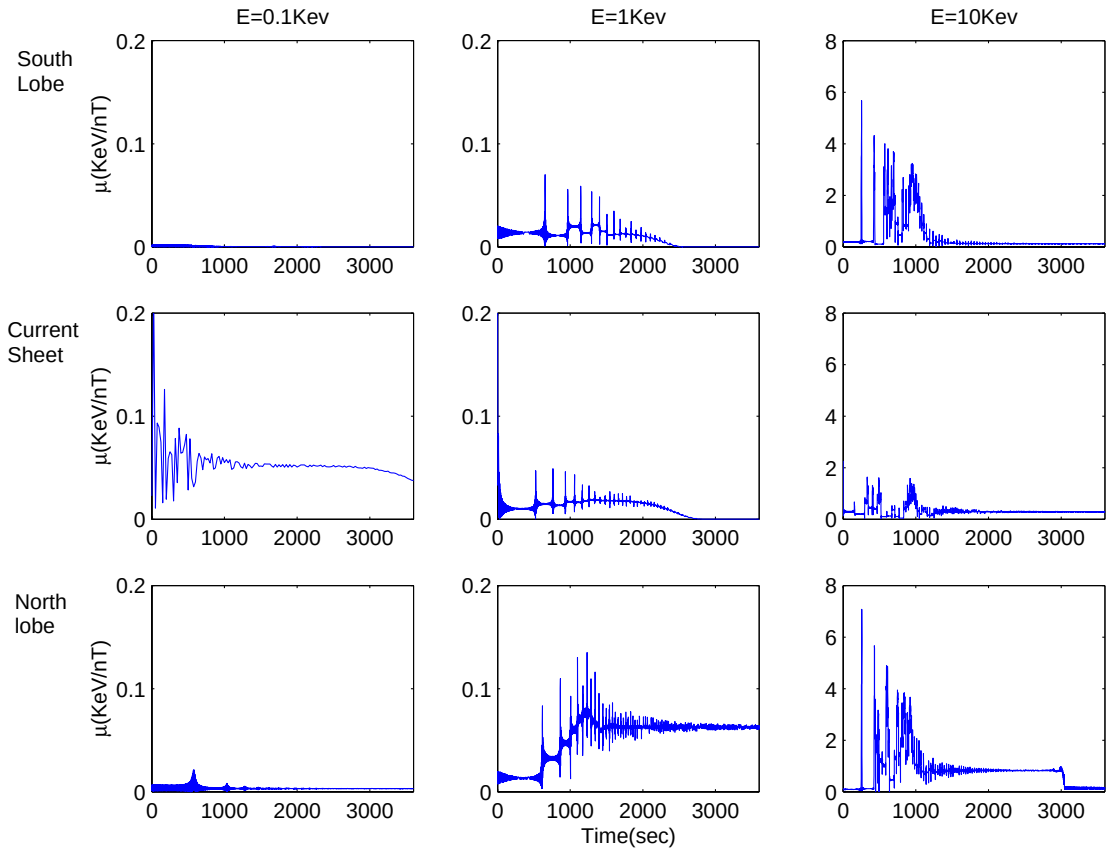

Figure 5.6: These plots are the magnetic moment μ versus time. The unit of the magnetic moment μ is $keV/$nT. The parameters are the same with previous figures.

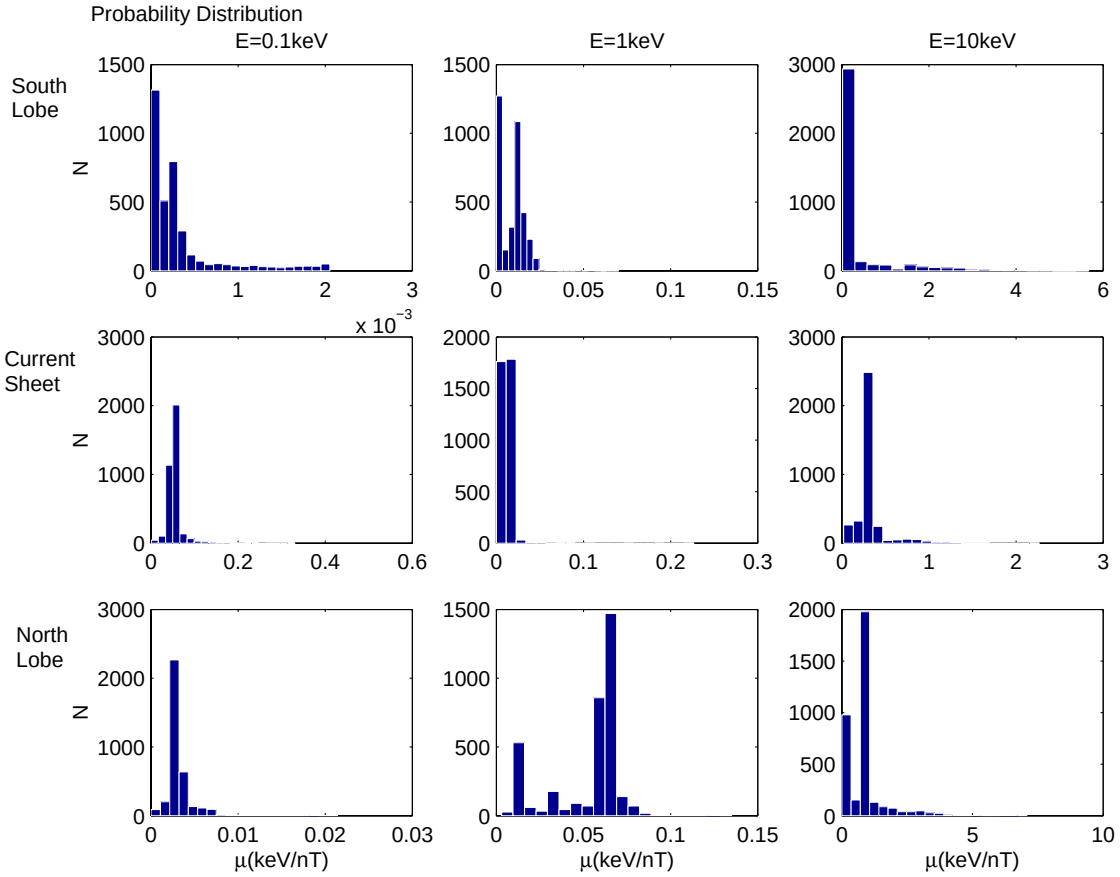

Figure 5.7: These plots are the distribution functions of the magnetic moment μ. The orbit time is a hour. The data is recorded in every second. The total number N of each plot is 3601. Figure 5.7 corresponds to figure 5.6.

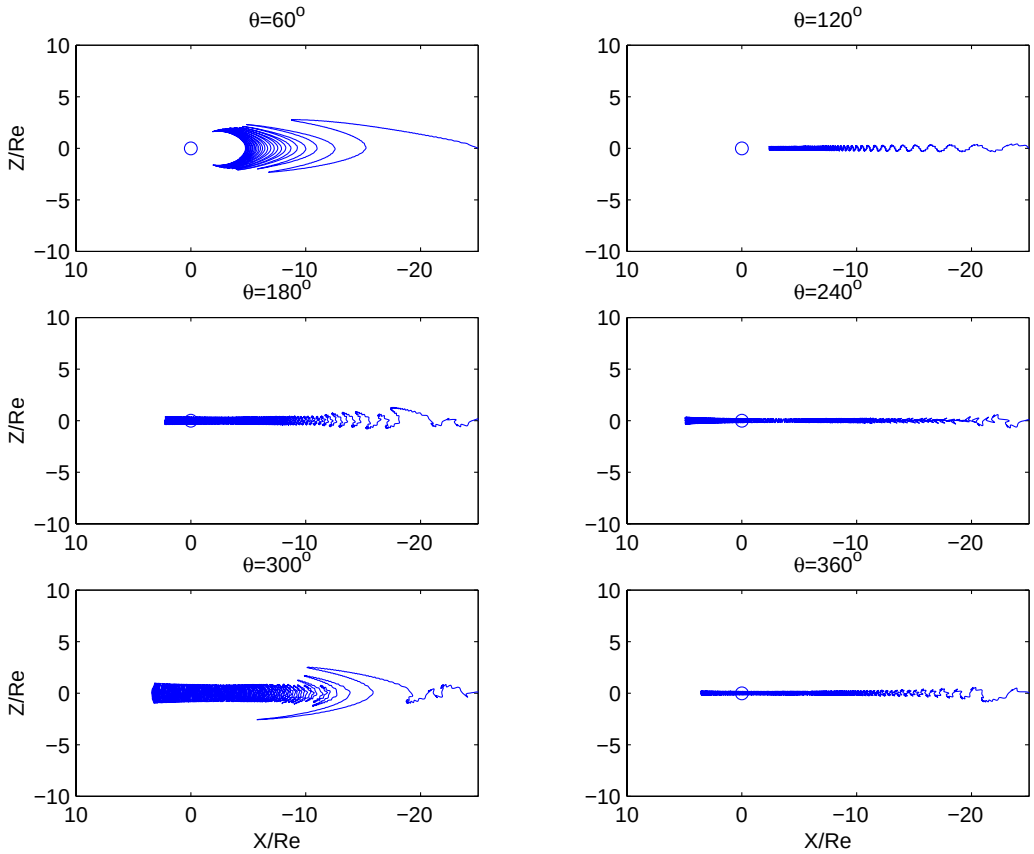

Figure 5.8: The particles drift in different gyrophase angle with the same proton energy $1keV$. The gyrophase angle starts from 60° to 360°. The interval angle is 60°. Particles drift 3600 seconds (a hour). The parameters of the Tsyganenko 96 model are the same with the ones in figure 5.2. These figures are shown in meridian plane.

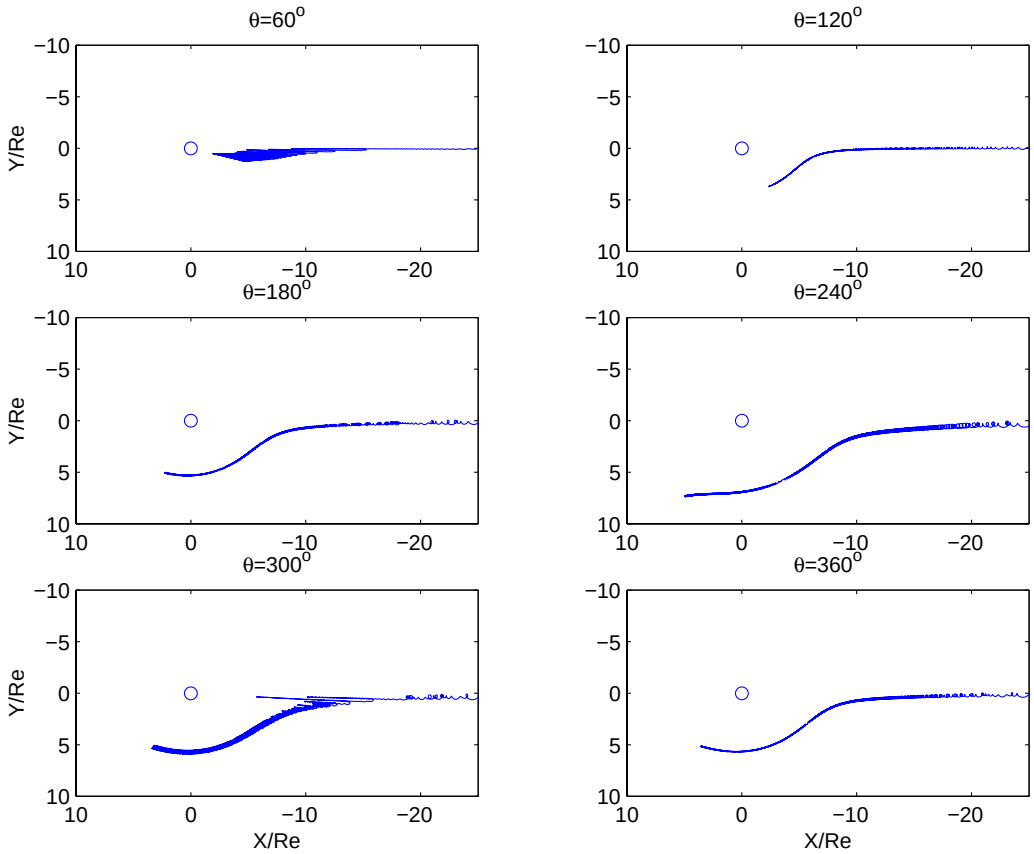

Figure 5.9: These plots are shown in equatorial plane. The parameters of the Tsyganenko 96 model are the same with the ones in figure 5.2. The line connected gyrophase angle 180° with 360° divide the equatorial plane into two parts, dayside and nightside. The gyrophase angle 60° and 120° are located in the dayside; 240° and 300° are located in the nightside.

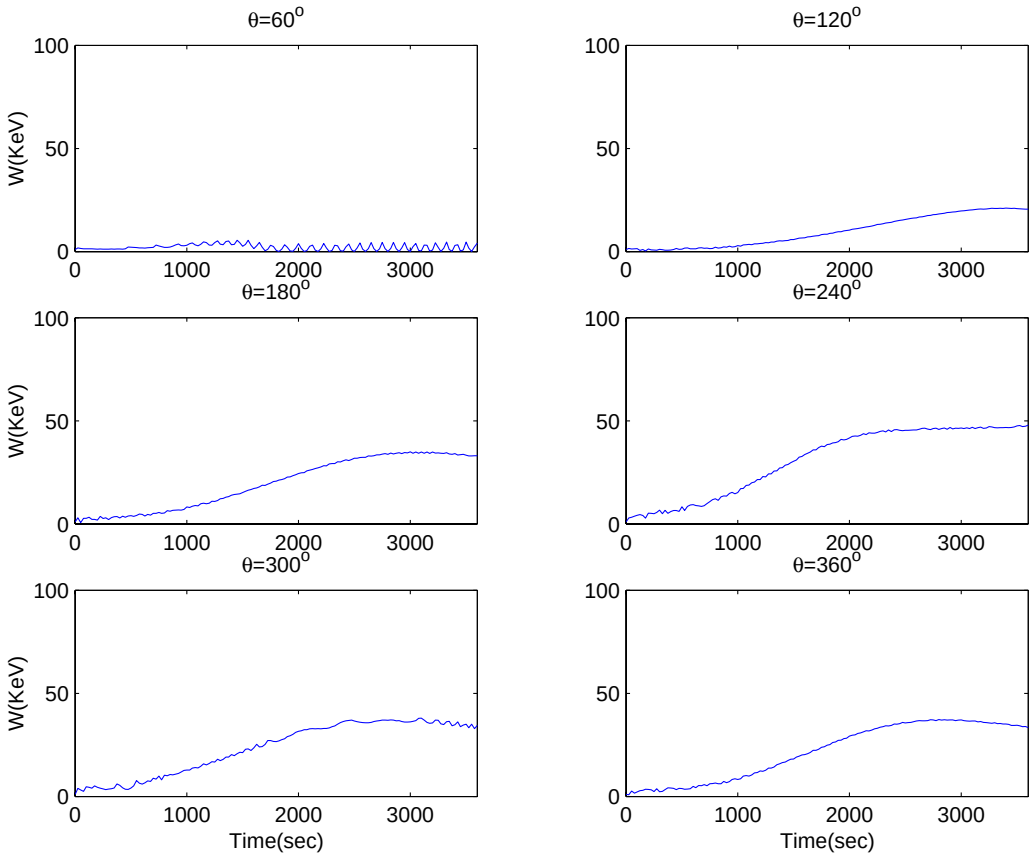

Figure 5.10: These plots are the total energy calculated from equation (2) versus time. The parameters of the Tsyganenko 96 model are the same with the ones in figure 5.2. The unit of total energy is expressed in keV. The interval gyrophase angle is 60°.

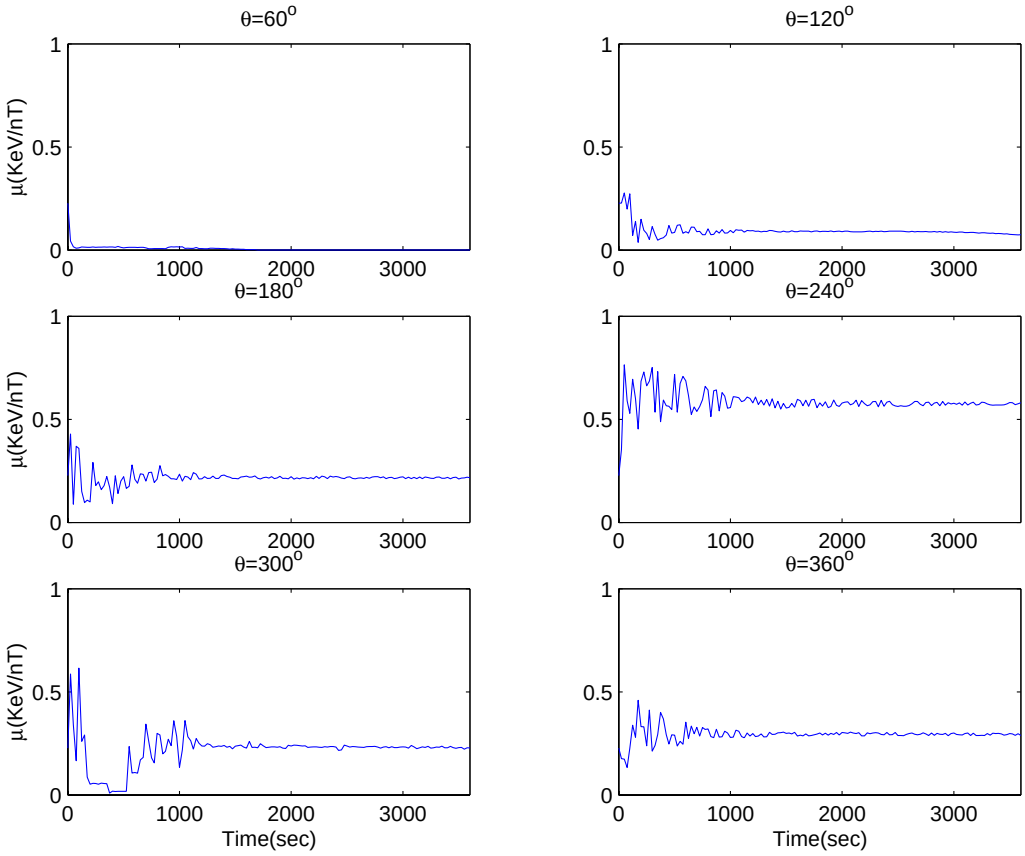

Figure 5.11: These plots are the magnetic moment μ versus time. The parameters of the Tsyganenko 96 model are the same with the ones in figure 5.2. The interval of gyrophase angle is 60°.

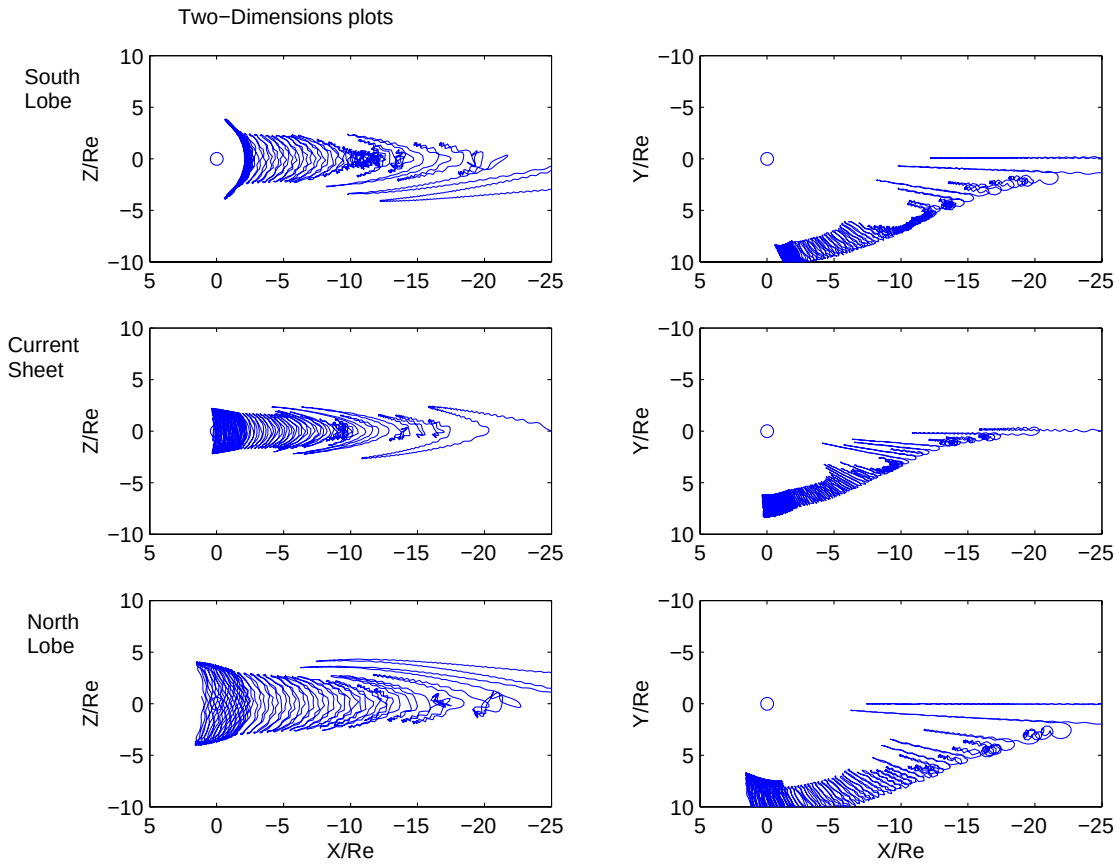

Figure 5.12: The initial conditions of the particles are shown in table 5.2. The particles start to drift from three different positions, current sheet, north lobe and south lobe. The electric field changes to the opposite direction after 30 minutes. The first column figures are shown in meridian plane; the second column plots are shown in equatorial plane.

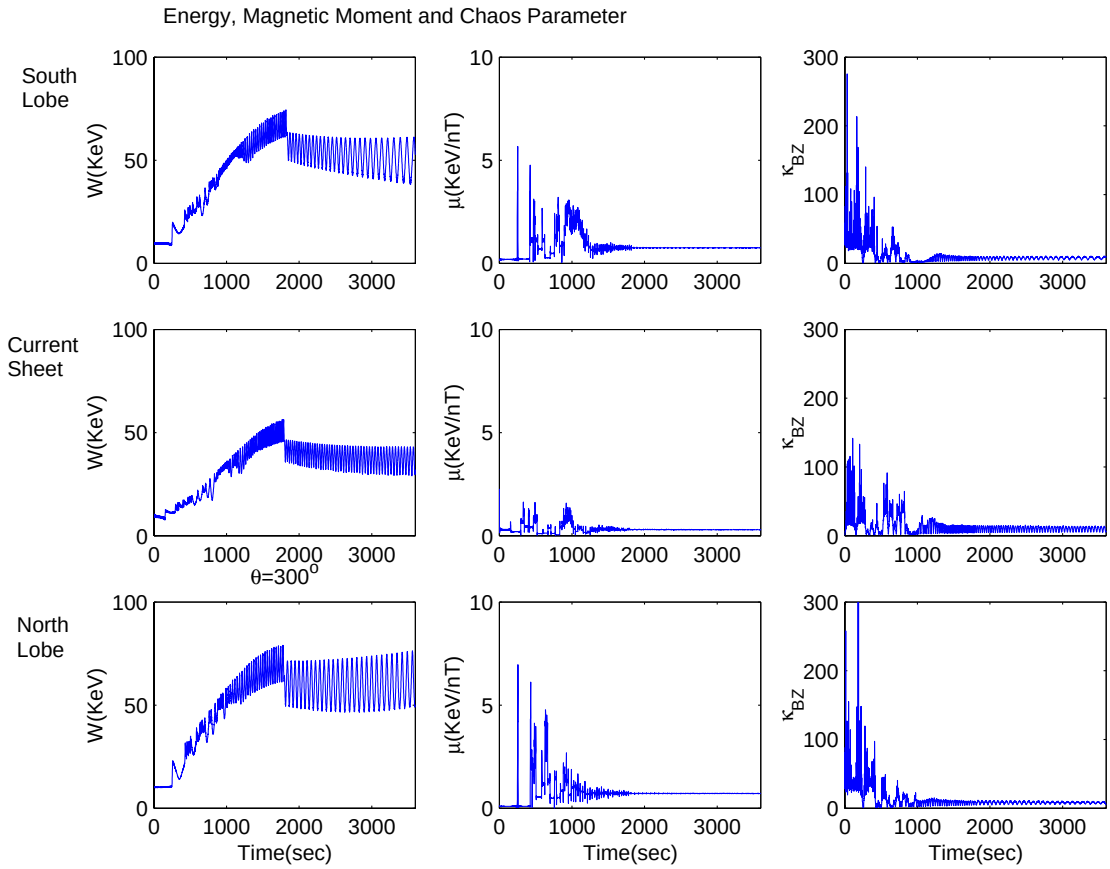

Figure 5.13: The first column figures are the energy from equation (5.2) versus time. The second column figures are the magnetic moment μ versus time. The rest plots in the last column are the chaos parameterκ_{BZ} versus time. The initial conditions of these figures are shown in table 5.2.

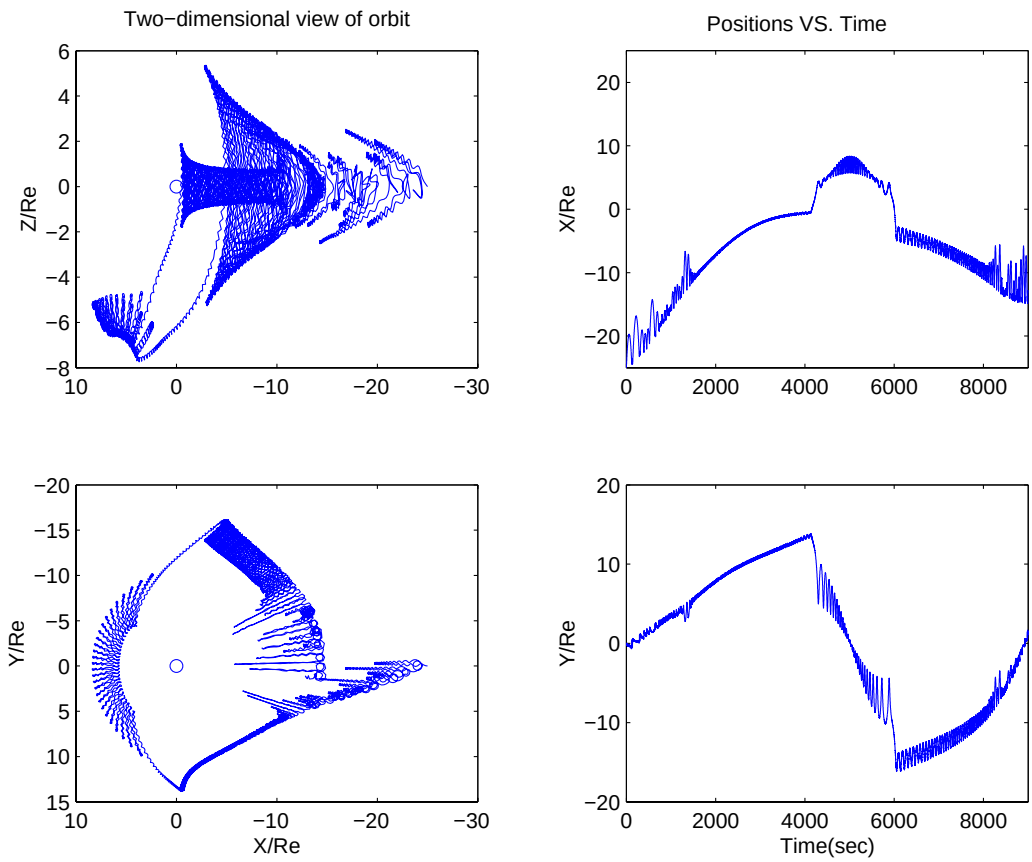

Figure 5.14: The left column figures are shown in meridian plane and equatorial plane. The right column plots show positions in x-axis and y-axis versus time.

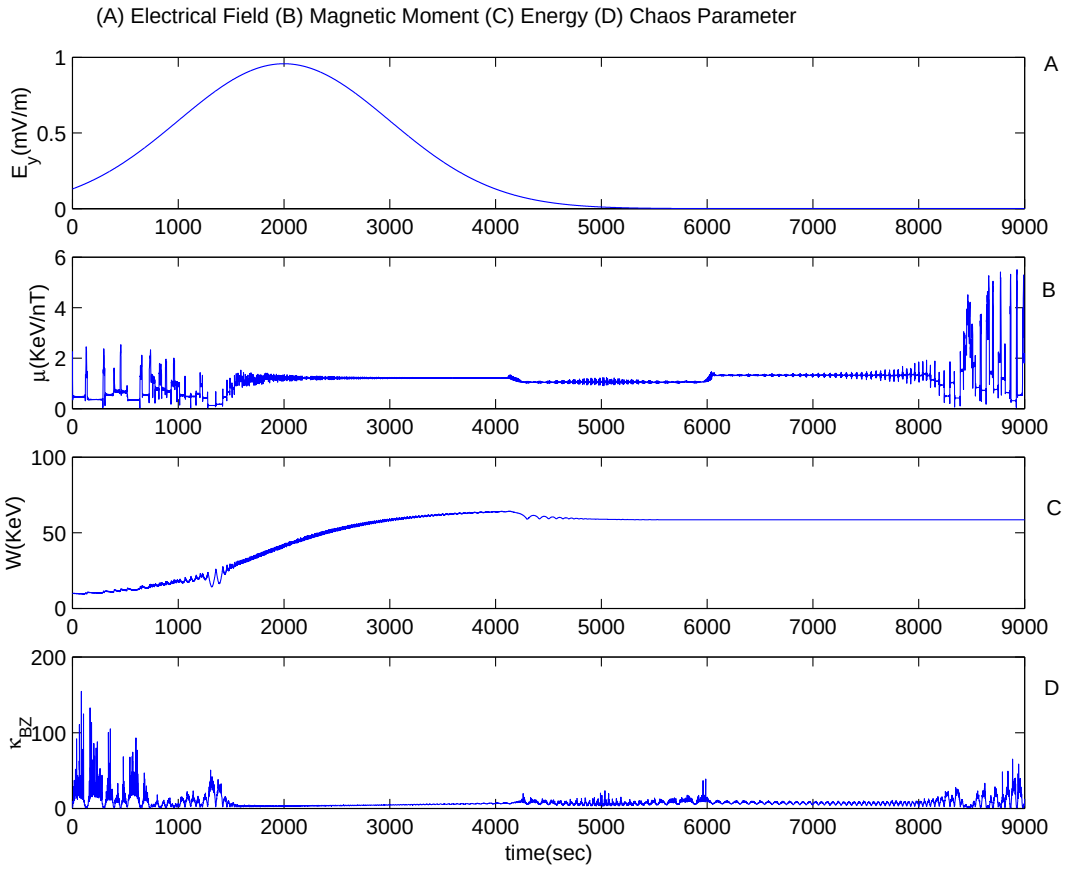

Figure 5.15: These plots display the electric field, the magnetic moment μ, energy and chaos parameter κ_{BZ} versus time. The electric field is the Gaussian distribution calculated from equation 5.5.

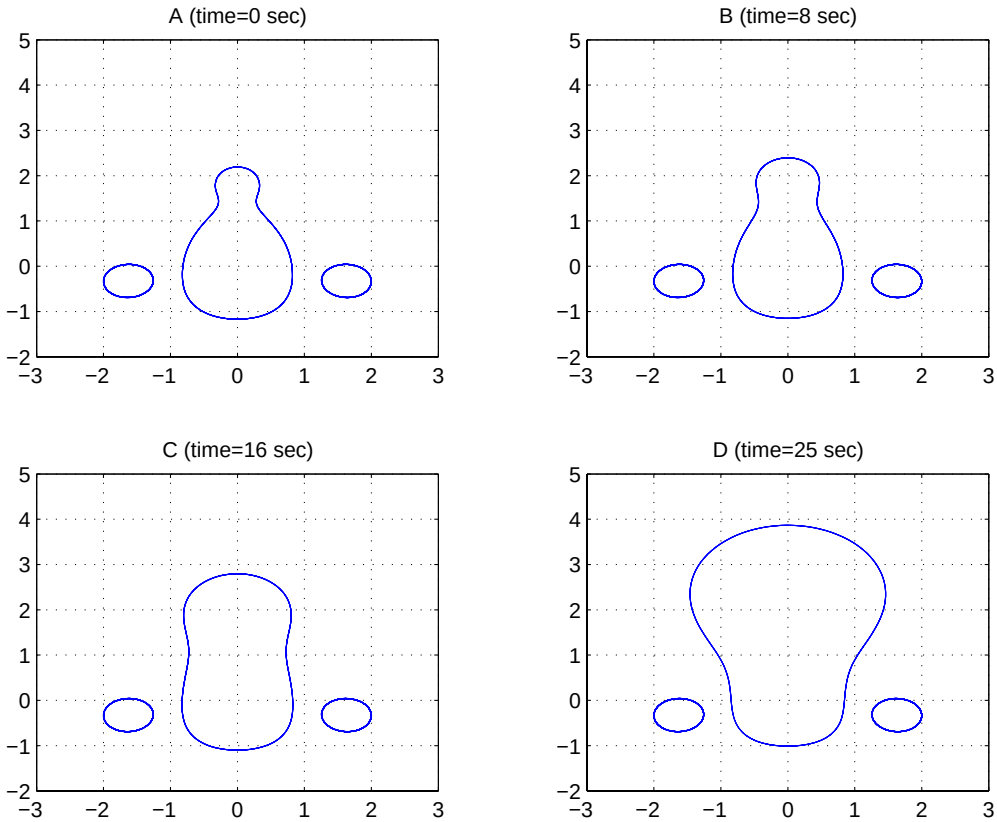

Figure 5.16: Simple emerging flux current model is $\mathrm{sech}(2\pi t/100)$ for the strength of the two line dipoles in equation (1). Plots show the time is 0, 8, 16 and 25 second respectively. The dipoles are below the photospheric surface at $y = -0.3L_\circ$ and centered at $x = \pm 0.3$ and $\pm 1.5L_\circ$. The maximum flux $(\mu_\circ I/2\pi)$ is 10^6 wb/m

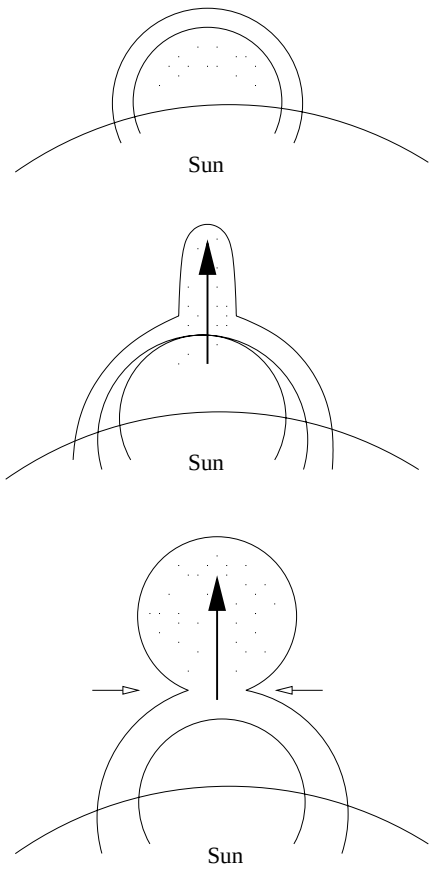

Figure 5.17: At the initial moment all particles are within the solar magnetic field. When the magnetic field starts to reconnect, particles erupt to the outer magnetic field and make a self-organized coherent structure. The size of the structure is around $4 \times 10^{15} km^3$ with energy about $10^{23} J$.

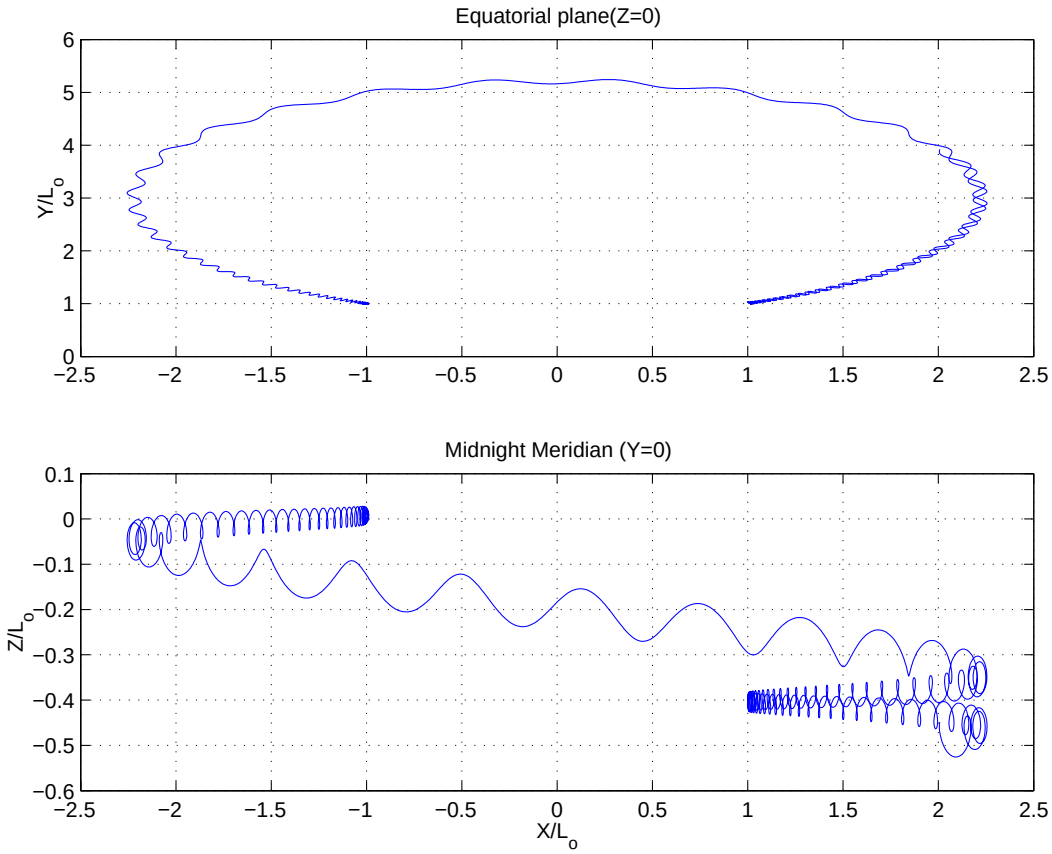

Figure 5.18: The particle does the mirror motion in this simple emerging current model sech($2\pi t/100$). The top plot is in the equatorial plane($z = 0$); the bottom one is in the Midnight Meridian($y = 0$).

Chapter 6

Results and Conclusions

The objective of this thesis was to look for the energy gain mechanism of a charged particle drifting in the geomagnetic tail under different electric fields. This may also be stated as searching for the acceleration region of the charged particles. In Chapter 4 the chaos parameter κ_{BZ} has the strong variations when the magnetic moment μ is not conserved. Guiding center approximations work before and after the particles cross the neutral sheet. Under the good adiabatic condition the chaos parameter κ_{BZ} is larger than 2. The magnetic moment μ is not constant and the chaos parameter κ_{BZ} drops below 2 when the particles cross the neutral sheet. We can use the standard map to know the change of the magnetic moment μ over long time. These considerations lead to an estimate of the energy which is released into the ring current.

In Chapter 5 the ions spend 30 minutes drifting close to the Earth around $5R_E$ and gain the energy around $50keV$ wherever particles start to drift from the north lobe, the south lobe or the current sheet at the same yz plane in the geotail when the constant electric field $E_y = 1mV/m$. The

particles drift to the evening sector and start to release the energy into ring current. The particles release around $10keV$ into the ring current under the constant electric field $1mV/m$. The magnetic moment μ changes when the particles cross the neutral sheet. Then the particles drift to the noon side of the Earth.

The different electric field models can influence how much energy ions gain or drop. Under a variable electric field from equation (5.5), the ions starting to drift from the geotail drift to the dusk sector of the Earth. Then ions pass the dusk area and drift slowly in the noon area and then drift back to the geomagnetic tail region through the dawn side of the Earth. The particles gain the energy around $50keV$. The particles release the energy around $5keV$ as they float in the noon area. When the particles drift in the noon side the energies of particles do not change sharply. The particles drift back to the near-tail area of the Earth's magnetosphere. The particles gain and release the energy until the particles enter the Earth's ionosphere. A future project would be to launch ensembles of particles and attempt to predict the fraction that enter the ionosphere.

In section 5.4, I use the coronal magnetic field to simulate the charged particle motion in the atmosphere of the Sun. It is difficult to estimate the dissipated energy in a short time scale because of the Reynolds number $R_m \gg 1$. The solar particle within the corona performs the gyromotion and mirrors

back to the coronal magnetic configuration. This orbit is similar to the particle orbits in the Earth's geotail. The solar particles possess the giant energies as drifting away the Sun with coronal mass ejections. Through quick reconnection of the coronal magnetic field the particles in the corona are released into the space along with the spiral motion. Reconnection model is applied to numerical simulation in the solar flares and magnetospheric substorms.

In future work the behaviors of large ensembles of particles are needed. This thesis aims to show the prototype behavior of interesting particles by studying single charged particle orbits. We can employ parallel computing methods to estimate the behaviors of clouds of particles responding to the time dependent geotail fields at the same moment.

Appendices

Appendix A

Coordinate Transformation

Matrix arithmetic can be used to transfer coordinate as described by Russell [20]. We can transform from either GSE to GSM coordinate or from GSM to GSE coordinate. Each vector $\mathbf{X_2}$ can be transferred into $\mathbf{X_1}$ through transformation matrix $\mathbf{A}$ such that $X_1 = AX_2$. This formula can be written as follow:

$$\begin{bmatrix} x_1 \\ y_1 \\ z_1 \end{bmatrix} = \begin{bmatrix} a_{11} & a_{12} & a_{13} \\ a_{21} & a_{22} & a_{23} \\ a_{31} & a_{32} & a_{33} \end{bmatrix} \begin{bmatrix} x_2 \\ y_2 \\ z_2 \end{bmatrix} \tag{A.1}$$

Therefore, this question is simplified into a linear algebra question. There are several benefits using this method:[10]

1. It increases the calculating speed when doing the transformation of coordinates because there are three equations and three unknowns. It doesn't need to calculate trigonometric functions.

2. Transpose of transformation matrix (A^T) is easily found. The inverse matrix(A^{-1}) is also simply calculated. It is simple to utilize the calcu-

lations of linear algebra because axes of coordinate systems are linear independent respectively.

3. Transformation matrix can be decomposed into at least two matrices. On the other hand, it can be transferred into transitional matrix. For example, system A transferred into system C could be applied by a intermediate system B. This method is to multiply two matrices to get a transformation matrix $A_{ac} = A_{ab}A_{bc}$.

New X, Y and Z axes can be written in the old coordinate in equation (A.1) above

$$\begin{aligned} X &= (a_{11}, a_{12}, a_{13}) \\ Y &= (a_{21}, a_{22}, a_{23}) \\ Z &= (a_{31}, a_{32}, a_{33}). \end{aligned} \tag{A.2}$$

Appendix B

Model Fitting to Data Based Models

Using the least squares solution can find the estimate parameters when the values minimize residuals by making their sum a minimum. [**?**] Parameters are chosen to minimize the following performance index ε, which is the sum of squares of deviations:

$$\varepsilon = \sqrt{\sum_{i=1}^{n}((B_x^C - B_x^T)^2 + (B_z^C - B_z^T)^2)}, \tag{B.1}$$

for n samples of the original satellite data or the synthesized satellite data contained in the Tsyganenko 96 model values that parameter is the datum. In equation (B.1) $B_{x,z}^C$ is the CCM model field and B^T the data taken from Tsyganenko 96 model. We re-express the CCM as:

$$B_x^C = A_1 - 2A_3\frac{xz}{(x^2+z^2)^2} \tag{B.2}$$

$$B_z^C = A_2 + A_3\frac{x^2-z^2}{(x^2+z^2)^2} \tag{B.3}$$

in terms of the components $A_1 = B_x'$, $A_2 = B_n$ and $A_3 = B_o r_o^2$ where $\mathbf{A}$=(A_1, A_2, A_3) from the parameter vector describing the state of the geotail. In equation (B.1) n is the number of data points taken from the Tsyganenko

96 model to determine A_1, A_2 and A_3. Superscripts C and T mean Constant Current Model and Tsyganenko 96 model respectively. B_x^T and B_z^T are given through Tsyganenko 96 model or space flight data if available. In order to minimize the error function ε, it is necessary to satisfy two conditions as follows:

$\frac{\partial \varepsilon}{\partial A_i} = 0$ The equation gives the determinant set of equation for A_i. But it is still needed to look at the second derivatives to identify whether this solution set is minimum or not.

$|\frac{\partial^2 \varepsilon}{\partial A_i \partial A_j}| > 0$ Larger than zero means positive definite. It implies this solution set is the minimum of J.

Taking the derivate of error function ε with respect to A_i we find the minimum error conditions

$$\frac{\partial \varepsilon}{\partial A_1} = A_1 \sum_{i=1}^{n} z^2 - 2A_3 \sum_{i=1}^{n} \frac{xz^2}{(x^2+z^2)^2} - \sum_{i=1}^{n} B_x^T z = 0 \tag{B.4}$$

$$\frac{\partial \varepsilon}{\partial A_2} = A_2 \sum_{i=1}^{n} 1 + A_3 \sum_{i=1}^{n} \frac{x^2 - z^2}{(x^2+z^2)^2} - \sum_{i=1}^{n} B_z^T = 0 \tag{B.5}$$

$$\begin{aligned} \frac{\partial \varepsilon}{\partial A_3} = & A_1 \sum_{i=1}^{n} \frac{-2xz^2}{(x^2+z^2)^2} + A_2 \sum_{i=1}^{n} \frac{x^2 - z^2}{(x^2+z^2)^2} + A_3 \sum_{i=1}^{n} \frac{1}{(x^2+z^2)^2} \\ & - \sum_{i=1}^{n} \frac{-2B_X^T xz}{(x^2+z^2)^2} - \sum_{i=1}^{n} \frac{B_z^T (x^2 - z^2)}{(x^2+z^2)^2} = 0. \end{aligned} \tag{B.6}$$

There are three equations and three unknowns. It can be rewritten as $\mathbf{TX}=\mathbf{Q}$, where $\mathbf{X}=(A_1, A_2, A_3)$. $\mathbf{T}$ is the 3×3 matrix composed of the coefficients of A_1, A_2 and A_3. Therefore, the optimal value of A_1, A_2 and A_3 can be estimated by linear algebra. The curvature ε'' can be written as:

$$\frac{\partial^2 \varepsilon}{\partial A_i \partial A_j} = \begin{bmatrix} \sum_{i=0}^{n} z^2 & 0 & \sum_{i=0}^{n} \frac{-2xz^2}{(x^2+z^2)^2} \\ 0 & n & \sum_{i=0}^{n} \frac{x^2-z^2}{(x^2+z^2)^2} \\ \sum_{i=0}^{n} \frac{-2xz^2}{(x^2+z^2)^2} & \sum_{i=0}^{n} \frac{x^2-z^2}{(x^2+z^2)^2} & \sum_{i=0}^{n} \frac{1}{(x^2+z^2)^2} \end{bmatrix}, \tag{B.7}$$

where n means there are n data points. ε'' is larger than zero at each point in the night-side region. For data obtaining from Tsyganenko 96 model with parameters $P_{dyn} = 3.0\text{nT}$, $D_{st} = -50\text{nT}$, $B_Y^{IMF} = 0.0\text{nT}$, $B_Z^{IMF} = 10.0$ nT, the setting parameters of Constant Current Model are $B'_x \approx 14.671\text{nT}(R_E)$, $B_n \approx -0.0001021\text{nT}$ and $B_o r_o^2 = 6579.6\text{nT}(R_E)^2$. Constant Current Model in figure 3.1 comes from model-fitting of Tsyganenko 96 model in the top plot of figure 3.1. With these parameters at (-5.0, 0.0, 1.0) the ε is 122.1 and ε'' are

$$\begin{bmatrix} 1 & 0 & 0.015 \\ 0 & 1 & 0.036 \\ 0.015 & 0.036 & 0.0015 \end{bmatrix}. \tag{B.8}$$

Index

Bibliography

[1] H. Alfvén and Carl-Gunne Fälthammar. *Cosmical Electro-dynamics: Fundamental Principles.* Oxford University Press, 1963.

[2] F. F. Chen. *Introduction to plasma physics and controlled fusion. Volume 1: Plasma Physics.* Plenum Press, 1984.

[3] P. F. Chen and K. Shibata. An emerging flux trigger mechanism for coronal mass ejections. *The Atmosphys. J.*, 545:524–531, 2000.

[4] C. Crabtree. *Ballooning stability of Earth's Magnetosphere.* PhD thesis, The University of Texas at Austin, 2003.

[5] D. C. Delcourt and R. F. Martin Jr. Application of centrifugal impulse to particle in the near-earth magnetotail. *J. Geophys. Res.*, 99:23583–23590, 1994.

[6] C. Crabtree *et al.* Bounce-averaged stability of compressional models in geotail flux-tubes. *J. Geophys. Res.*, 108:1084–1105, 2003.

[7] H. V. Wong *et al.* Low frequency stability of geotail plasma. *Phys. Plasma*, 8:2415–2424, 2001.

[8] W. Horton *et al.* Stability properties of high-pressure geotail flux tubes. *J. Geophys. Res.*, 106:18803–18822, 2001.

[9] R. J. Glodston and P. H. Rutherford. *Introduction to Plasma Physics.* Institute of Physics Publishing, 1995.

[10] M. A. Hapgood. Space physics coordinate transformations: A user guide. *Planet. Space Sci.*, 40:711–717, 1992.

[11] R. D. Hazeltine and F. L. Waelbroeck. *The Framework of Plasma Physics.* Persues Books, 1998.

[12] W. Horton and I. Doxas. A low-dimensional energy-conserving state space model for substorm dynamics. *J. Geophys. Res.*, 101:27223–27237, 1996.

[13] W. Horton and Y-H Ichikawa. *Chaos and Structures in Nonlinear Plasma.* World Science Press, 1996.

[14] W. Horton and T. Tajima. Decay of correlations and the collisionless conductivity in the geomagnetic tail. *Geophys. Res. Letters.*, 17:123–126, 1990.

[15] W. Horton and T. Tajima. Transport from chaotic orbits in the geomagnetic tail. *Geophys. Res. Letters.*, 18:1583–1586, 1991.

[16] A. J. Hundhausen. The origin and propagation of coronal mass ejections, proceedings of the sixth international solar wind conference, edited by v. j. pizzo, t. e. holzer and d. g. sime. Technical Report 306, National Cneter for Atmos. Pes., Boulder, Colo, 1988.

[17] R. L. Kaufmann and C. Lu. Cross-tail current: Resonant orbits. *J. Geophys. Res.*, 98:15447–15465, 1993.

[18] D. J. Larson. *Cross-tail current carriers in a two-dimension equilibrium magnetotail model.* PhD thesis, University of New Hampshire, 1996.

[19] C. E. McIlwain. Coordinates for mapping the distribution of magnetically trapped particles. *J. Geophys. Res.*, 66:3681–3691, 1961.

[20] C. T. Russell. Geophysical coordinate transformation. *Cosmic Electrodyn.*, 2:184–196, 1971.

[21] C. T. Russell and M. G. Kivelson. *Introduction to Space Physics.* Cambridge University Press, 1995.

[22] B. K. Teo and G. Raithel. Atom reflection in a tapered magnetic guide. *Phys. Rev. A*, 65:051401:1–4, 2002.

[23] N. A. Tsyganenko. On the convective mechanism for formation of the plasma sheet in the magnetospheric tail. *Planet. Space Sci.*, 30:1007–1012, 1982.

[24] N. A. Tsyganenko. Global quantitative models of geomagnetic field in the cislunar magnetosphere for different disturbance levels. *Planet. Space Sci.*, 35:1347–1358, 1987.

[25] N. A. Tsyganenko. A magnetospheric magnetic field model with warped tail current sheet. *Planet. Space Sci.*, 37:5–20, 1989.

[26] N. A. Tsyganenko. Modeling the earth's magnetospheric magnetic field confined within a realistic magnetopause. *J. Geophys. Res.*, 100:5559–5612, 1995.

[27] N. A. Tsyganenko and Stern D, P. Modeling the global magnetic field of the large-scale birkkeland current systems. *J. Geophys. Res.*, 101:27187–27198, 1996.

[28] N. A. Tsyganenko and M. Peredo. Analytic models of the magnetic field of disk-shaped current sheets. *J. Geophys. Res.*, 99:199–205, 1994.

[29] N. A. Tsyganenko and A. V. Usmanov. Determination of the magnetospheric current system parameters and development of experimental geomagnetic field models based on data from imp and heos satellites. *Planet. Space Sci.*, 30:985–998, 1982.

Vita

Wei-Tai Lin was born on August 15, 1976 in Taipei, Taiwan. He was admitted into National Central University in Taoyuan, Taiwan through a competitive entrance examination in 1994. He majored in Space Science in Department of Atmospheric Science and obtained the degree of Bachelor of Science in 1998.

After graduating from National Central University, he joined the Air Force to fulfill the required military service. During a two-year period, he was commissioned as a second lieutenant and responsible for air management in Taoyuan airport. Later on he was employed by ROCSAT-1 research group in Academia Sinica to filter and analyse the data observed from ROCSAT-1. ROCSAT-1 is the first satellite of Taiwan.

He came to the United States in July 2001 to start his graduate career at the University of Texas at Austin under the Pre-Emptive Fellowship. He expects to be granted the Master of Science in Electrical Engineering in December, 2003.

Permanent address: 3F NO. 7 LN. 7 Tahsin St. Hsintien, Taipei,
23106, Taiwan

This thesis was typeset with LaTeX[†] by the author.

[†]LaTeX is a document preparation system developed by Leslie Lamport as a special version of Donald Knuth's TeX Program.